Robotica: (2020) volume 38, pp. 69–87. © Cambridge University Press 2019
doi:10.1017/S026357471900047X

High-Gain Observer-Based Neural Adaptive Feedback Linearizing Control of a Team of Wheeled Mobile Robots

Neda Sarrafan† and Khoshnam Shojaei†‡*

†*Department of Electrical Engineering, Najafabad Branch, Islamic Azad University, Najafabad, Iran. E-mail: sarrafan.neda@gmail.com*
‡*Smart Microgrid Research Center, Najafabad Branch, Islamic Azad University, Najafabad, Iran*

(Accepted March 3, 2019. First published online: April 11, 2019)

SUMMARY
This paper addresses the neural network (NN) output feedback formation tracking control of non-holonomic wheeled mobile robots (WMRs) with limited voltage input. A desired formation is achieved based on the leader–follower strategy utilizing hyperbolic tangent saturation functions to reduce the risk of actuator saturation. The controller is developed by incorporating the high-gain observer and radial basis function (RBF) NNs using the inverse dynamics control technique. The high-gain observer is introduced to estimate velocities of the followers. The RBF NN preserves the robustness of the proposed controller against uncertain nonlinearities. The adaptive laws are also combined by a robust control term to estimate the weights of RBF NN, approximation errors, and bounds of unknown time-variant environmental disturbances. A Lyapunov-based stability analysis proves that all signals of the closed-loop system are bounded, and tracking errors are uniformly ultimately bounded. Finally, some simulations are carried out to show the effectiveness of the proposed controller for a number of WMRs.

KEYWORDS: Actuator saturation; Adaptive robust control; High-gain observer; Leader– follower formation; Radial basis function neural network; Wheeled mobile robots.

1. Introduction

The motion control of wheeled mobile robots (WMRs) is an attractive research area due to the challenging theoretical nature of underactuated systems. Over the last few years, the cooperative and formation control of multiple autonomous mobile vehicles has been a subject of considerable research efforts due to the redundancy, robustness, and efficiency of vehicle teamwork with respect to a single robot. The formation control of wheeled mobile vehicles can be efficiently employed in various applications, such as the exploration, surveillance, security patrols, search, rescue, and various military missions. Various control strategies for mobile robot formations can be divided into three major approaches, namely behavior-based formation control,[1,2] virtual structure method,[3,4] and leader–follower approaches.[5,6] Among them, the leader–follower architecture has been widely used due to its simplicity, scalability, and reliability.

One of the pioneering leader–follower-based controllers was introduced by Desai *et al.* in 1998.[7] Most of the current researches based on this approach only considered the kinematic model of mobile robots, which require the perfect velocity tracking assumption.[8,9] It is noteworthy that the controller design based on a kinematic model has an acceptable performance only at low speeds and when the robot is not under high loads. Hence, many leader–follower formation control design methods[10–13] considered the nonlinear dynamical model to improve the performance of the controller. As shown in

* Corresponding author. E-mail: khoshnam.shojaee@gmail.com

ref. [14], a traditional model-based adaptive controller was designed using the inverse dynamics technique for a single WMR. However, it is generally useful only for systems in which the dynamics are linear-in-parameters. Just as described in refs. [10–13], the proposed approximation-based control techniques, such as fuzzy, neural network (NN), optimal, model predictive, and robust controllers, were developed to compensate functional uncertainties and unknown time-varying environmental disturbances. It should be pointed out that most of the previously presented controllers require velocity measurements of all agents that are not easily measurable because of noise contamination and communication delays. Moreover, from a practical viewpoint, velocity sensors like tachometers may increase the implementation cost and weight of the system. One powerful solution to leave out velocity sensors is the design of output feedback controllers. Towards this end, the output feedback control schemes were designed for mobile robots in different works, including refs. [15–23], which is very demanding due to the nonholonomic constraints. Furthermore, the existence of parametric and nonparametric uncertainties in the kinematic and dynamic models of mobile robots makes this problem more challenging. In ref. [15], an output feedback controller was developed for the dynamic model of a unicycle-type mobile robot using a coordinate transformation in order to cancel the velocity cross terms in the WMR dynamics. It was, however, assumed that all parameters must be known. In refs. [19–23], the output feedback formation controllers were proposed in the presence of model uncertainties. Besides the previous works, the high-gain observer technique, which was first proposed by Khalil *et al.* in ref. [24], has evolved into an important tool to reach the output feedback control of uncertain nonlinear systems.[25,26] It can estimate the time derivatives of the system output by properly adjusting gains of the proposed observer. The actuator input constraint is also one of the major problems that occur in the control of actuated dynamic systems. Most of the presented works, including output feedback controllers,[15–23] assume that WMR actuators are capable of accepting every level of voltage signals. The main challenge usually arises when a large amplitude of the control signal is required to obtain a good tracking performance of hard reference trajectories, which can cause saturation of actuators. Therefore, it may lead to serious physical damages, thermal or mechanical damages of robot actuators. This problem can be alleviated by employing saturation functions to the design of tracking controller. Motivated by the above literature review, main contributions of this paper are stated as follows:

(i) In this paper, a neural adaptive output feedback linearizing formation control of WMRs is addressed for the first time. Compared with many previous works,[1–23] our proposed tracking controller does not require velocity measurements for real implementations by designing a high-gain observer.
(ii) In contrast to previously proposed controllers,[15–23] our presented output feedback formation controller takes the input constraint into account. For this purpose, the hyperbolic tangent saturation function is applied to the design of the inverse dynamic controller in order to bound the tracking error variables.
(iii) The proposed controller retains its robustness against uncertain parameters, external disturbances, and frictions by incorporating an RBF NN and an adaptive robust controller.

A Lyapunov-based stability analysis was used to prove that all signals in the closed-loop system are bounded and the position tracking errors are uniformly ultimately bounded (UUB). Finally, simulation results are provided for a number of WMRs to illustrate the efficiency of the proposed controller.

The rest of the paper is organized as follows. In Section 2, the problem statement is presented. In Section 3, main results of this paper, including the proposed adaptive robust neural output feedback formation controller design and its stability analysis, are presented. In Section 4, some numerical simulations are provided to evaluate the controller performance. Finally, conclusions are given in Section 5.

2. Problem Statement

2.1. Notations

Throughout this paper, $\|x\| := \sqrt{x^T x}$ is used as the Euclidean norm of a vector $x \in \Re^n$, while the induced norm of a matrix $A \in \Re^{n\times m}$ is defined as $\|A\| := \sqrt{\lambda_{\max}\{A^T A\}}$. The matrix I_n denotes

https://doi.org/10.1017/S026357471900047X Published online by Cambridge University Press

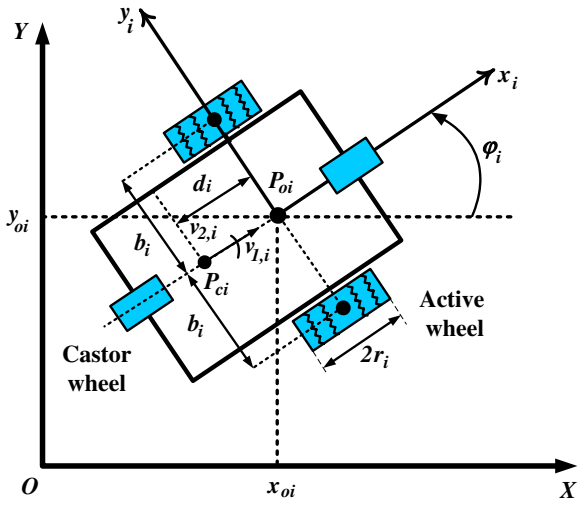

Fig. 1. A planar illustration of the WMR.

n-dimensional identity matrix. $\lambda_{\min}(\bullet)$ and $\lambda_{\max}(\bullet)$ denote the smallest and largest eigenvalues of a matrix, respectively. To facilitate control design and stability analysis, the following notations are also used: $Tanh(p_i) = (\tanh(p_{1i}), \ldots, \tanh(p_{ni}))^T$ and $Sech^2(p_i) = diag(\text{sech}^2(p_{1i}), \ldots, \text{sech}^2(p_{ni}))$, where $p_i = (p_{1i}, p_{2i}, \ldots, p_{ni})^T$; $diag(\bullet)$ denotes a diagonal matrix; $\tanh(\bullet)$ and $\text{sech}^2(\bullet) = 1/\cosh^2(\bullet)$ are hyperbolic tangent function and its derivative, respectively. Furthermore, the subscript i is used to represent the number of each follower in the group.

2.2. *WMR model description*

Consider a team of N identical nonholonomic unicycle-type mobile robots whose dynamic model is described, as follows, for ith robot according to Fig. 1:[27]

$$\dot{p}_i = G_i(p_i)v_i(t), \quad i = 1, 2, \ldots, N \tag{1}$$

$$M_i(p_i)\ddot{p}_i + C_i(p_i, \dot{p}_i)\dot{p}_i + B_i(p_i)F_i(\dot{p}_i) + B_i(p_i)\tau_{d_i} = B_i(p_i)\tau_i - A_i^T(p_i)\lambda_i \tag{2}$$

The posture of the ith robot is specified by $p_i = (x_i, y_i, \varphi_i)^T$, where (x_i, y_i) denotes the actual Cartesian position for the front of the robot and φ_i is the heading angle. $v_i(t) = (v_{1,i}(t), v_{2,i}(t))^T$ is made up of linear and angular velocities, respectively. Under the hypothesis of pure rolling and nonslipping conditions, each vehicle satisfies the nonholonomic constraint $A_i(p_i)\dot{p}_i = 0$, where $A_i(p_i) \in \Re^{1\times 3}$.[28] The full rank rotation matrix $G_i(p_i) \in \Re^{3\times 2}$ consists of smooth and linearly independent vector fields that are in the null space of $A_i(p_i)$, such that $A_i(p_i)G_i(p_i) = 0$. Moreover, $M_i(p_i) \in \Re^{3\times 3}$ is a symmetric positive definite inertia matrix, $C_i(p_i, \dot{p}_i) \in \Re^{3\times 3}$ is the centripetal and Coriolis matrix, $B_i(p_i) \in \Re^{3\times 2}$ is the input transformation matrix, $F_i(\dot{p}_i) \in \Re^{2\times 1}$ denotes the friction vector, $\tau_{d_i} \in \Re^{2\times 1}$ denotes the bounded unknown disturbances, $\tau_i \in \Re^{2\times 1}$ is the torque vector that is generated by wheel actuators, and $\lambda_i \in \Re$ is Lagrange multiplier that denotes constraint forces. The model matrices are defined as follows:

$$\begin{gathered} G_i(p_i) = \begin{pmatrix} \cos\varphi_i & 0 \\ \sin\varphi_i & 0 \\ 0 & 1 \end{pmatrix}, \; C_i(p_i, \dot{p}_i) = \begin{pmatrix} 0 & 0 & m_{ci}d_i\dot{\varphi}_i\cos\varphi_i \\ 0 & 0 & m_{ci}d_i\dot{\varphi}_i\sin\varphi_i \\ 0 & 0 & 0 \end{pmatrix}, \; B_i(p_i) = \frac{1}{r_i}\begin{pmatrix} \cos\varphi_i & \cos\varphi_i \\ \sin\varphi_i & \sin\varphi_i \\ b_i & -b_i \end{pmatrix} \\ M_i(p_i) = \begin{pmatrix} m_i & 0 & m_{ci}d_i\sin\varphi_i \\ 0 & m_i & -m_{ci}d_i\cos\varphi_i \\ m_{ci}d_i\sin\varphi_i & -m_{ci}d_i\cos\varphi_i & I_i \end{pmatrix}, \; A_i(p_i) = (\sin\varphi_i \; -\cos\varphi_i \; 0) \end{gathered} \tag{3}$$

where $m_i = m_{ci} + 2m_{wi}$ and $I_i = I_{ci} + 2I_{mi} + m_{ci}d_i^2 + 2m_{wi}b_i^2$ and all robot parameters are defined in Table I. To include actuator dynamics in (2), it is assumed that the robot wheels are driven by two similar brush DC motors with mechanical gears.[14] The dynamic model of DC motors can be represented

https://doi.org/10.1017/S026357471900047X Published online by Cambridge University Press

Table I. Definitions of WMR parameters and variables.

Parameter/variable	**Description**
r_i	Radius of each driving wheel
$2b_i$	Distance between two diving wheels of the robot
d_i	Distance between the center of mass P_{ci} of the robot and middle point P_{0i}
m_{ci}	Mass of the platform without the driving wheels and the rotors of DC motors
m_{wi}	Mass of each driving wheel plus the rotor of its motor
I_{ci}	Moment of inertia of the platform without the driving wheels and the rotors of the motors about a vertical axis through P_{ci}
I_{mi}	Moment of inertia of each wheel and the motor rotor about a wheel diameter
$K_{\tau i}$	Matrix of motor torque constants
R_{a_i}	Matrix of armature circuit resistance
L_{a_i}	Matrix of armature circuit inductance
K_{bi}	Matrix of back electromotive force constant
n_i	Gear box ratio
$\tau_{m_i} \in \Re^2$	Vector of torques generated by DC motor
$i_{a_i} \in \Re^2$	Vector of armature current
$u_{a_i} \in \Re^2$	Motor input voltage vector
$\dot{\theta}_{m_i}$	Angular velocity of the DC motor

by $\tau_{m_i} = K_{\tau i} i_{a_i}$ and $u_{a_i} = L_{a_i} di_{a_i}/dt + R_{a_i} i_{a_i} + K_{bi}\dot{\theta}_{m_i}$, where all parameters and variables are shown in Table I. By ignoring armature inductance and considering relations between torque and velocity before and after gears $\dot{\theta}_{m_i} = n_i\dot{\theta}_i$ and $\tau_i = n_i\tau_{m_i}$, the delivered torque to WMR wheels by the actuators is given by $\tau_i = K_{1i}u_{a_i} - K_{2i}\dot{\theta}_i$, where $K_{1i} = n_i K_{\tau i}/R_{a_i}$ and $K_{2i} = n_i K_{bi} K_{1i}$ are actuator parameters. By considering a transformation matrix $X_{T_i} \in \Re^{2\times 2}$ that transforms wheel velocity to pseudo-velocity vector, the input torque vector can be rewritten as:

$$\tau_i = K_{1i}u_{a_i} - K_{2i}X_{T_i}v_i \tag{4}$$

After substituting (4) into (2), one obtains:

$$M_i(p_i)\ddot{p}_i + C_i(p_i,\dot{p}_i)\dot{p}_i + B_i(p_i)F_i(\dot{p}_i) + B_i(p_i)\tau_{d_i} = B_i(p_i)(K_{1i}u_{a_i} - K_{2i}X_{T_i}v_i) - A_i^T(p_i)\lambda_i \tag{5}$$

By differentiating (1), one obtains $\ddot{p}_i = \dot{G}_i(p_i)v_i + G_i(p_i)\dot{v}_i$, which is replaced in (5); then, by multiplying both sides of (5) by $G_i^T(p_i)$, the following dynamic equation is achieved:

$$\bar{M}_i(p_i)\dot{v}_i(t) + \bar{C}_i(p_i,\dot{p}_i)v_i(t) + \bar{F}_i(\dot{p}_i) + \bar{\tau}_{d_i} = K_{1i}\bar{B}_i(p_i)u_{a_i}, \tag{6}$$

where $\bar{M}_i(p_i) = G_i^T M_i G_i$, $\bar{C}_i(p_i,\dot{p}_i) = G_i^T M_i \dot{G}_i + G_i^T C_i G_i + K_{2i}\bar{B}_i X_{T_i}$, $\bar{B}_i(p_i) = G_i^T B_i$, $\bar{F}_i(\dot{p}_i) = \bar{B}_i F_i$ and $\bar{\tau}_{d_i} = \bar{B}_i\tau_{d_i}$, which are defined as follows:

$$\bar{M}_i(p_i) = \begin{pmatrix} m_i & 0 \\ 0 & I_i \end{pmatrix},\ \bar{C}_i(p_i,\dot{p}_i) = \begin{pmatrix} 2K_{2i}/r_i^2 & m_{ci}d_i\dot{\varphi}_i \\ -m_{ci}d_i\dot{\varphi}_i & 2b_i^2K_{2i}/r_i^2 \end{pmatrix},\ \bar{B}_i(p_i) = \begin{pmatrix} 1/r_i & 1/r_i \\ b_i/r_i & -b_i/r_i \end{pmatrix} \tag{7}$$

Property 1: The bounding functions $\|G_i(p_i)\| \le g_{1i}$, $\bar{m}_{1i} \le \|\bar{M}_i(p_i)\| \le \bar{m}_{2i}$, $\|\bar{C}_i(p_i,\dot{p}_i)\| \le \bar{c}_{1i}\|v_i\|$, $\|\bar{\tau}_{d_i}\| \le \bar{\tau}_{1i}$, and $\|\bar{F}_i(\dot{p}_i)\| \le \bar{f}_{1i} + \bar{f}_{2i}\|v_i\|$ are valid for the presented kinematic and dynamic models of nonholonomic robots, where g_{1i}, $\bar{m}_{1i}$, $\bar{m}_{2i}$, $\bar{c}_{1i}$, $\bar{\tau}_{1i}$, $\bar{f}_{1i}$, and $\bar{f}_{2i}$ are positive scalar constants.[29]

2.3. State space representation

The kinematic model (1) and dynamic equation (6) may be combined into the following state space representation in companion form:

$$\dot{x}_i = \begin{pmatrix} \dot{p}_i \\ \dot{v}_i \end{pmatrix} = \underbrace{\begin{pmatrix} G_i(p_i)v_i \\ 0 \end{pmatrix}}_{f_i(x_i)} + \underbrace{\begin{pmatrix} 0 \\ -\bar{M}_i^{-1}\bar{C}_i(p_i,\dot{p}_i)v_i \end{pmatrix}}_{q_i(x_i)} + \underbrace{\begin{pmatrix} 0 \\ \bar{k}_{1i}\bar{M}_i^{-1}\bar{B}_i \end{pmatrix}}_{g_i(x_i)} u_{a_i} + \underbrace{\begin{pmatrix} 0 \\ -\bar{M}_i^{-1}(\bar{F}_i(\dot{p}_i) + \bar{\tau}_{d_i}) \end{pmatrix}}_{\Delta_i(x_i)}, \tag{8}$$

https://doi.org/10.1017/S026357471900047X Published online by Cambridge University Press

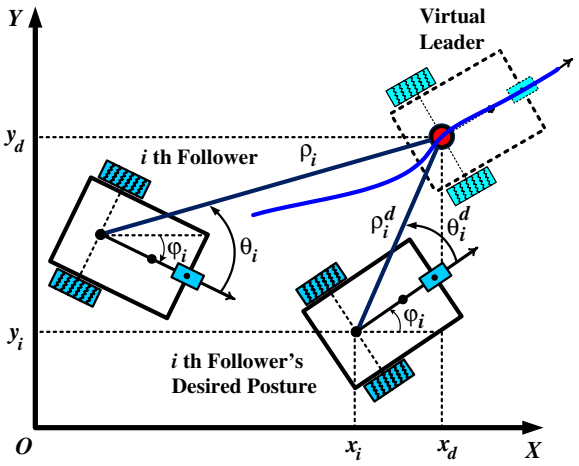

Fig. 2. A leader–follower formation control scheme.

where $x_i = (p_i^T, v_i^T)^T \in \Re^5$ is the state vector, and $f_i(x_i)$, $q_i(x_i)$, $g_i(x_i)$, $\Delta_i(x_i) \in \Re^5$ are smooth vector fields with $g_i(0) \neq 0$ for holding the controllability of the system. The trajectory tracking problem will be solved by applying differential geometric control theory based on this representation.

2.4. Control objectives and mathematical preliminaries

Definition 1. **[30]** *The solutions of $\dot{x} = f(t, x)$ are said to be UUB, if there exist positive constants b and c, independent of the initial condition $t_0 \geq 0$ and for every $a \in (0, c)$, there is a time $t_f \geq 0$ independent of t_0 such that if $\|x(t_0)\| \leq a$, then $\|x(t)\| \leq b$, for all $t \geq t_0 + t_f$.*

Definition 2. *Given a smooth bounded reference trajectory $p_d(t) = (x_d, y_d, \varphi_d)^T$, which is generated by an open-loop motion planner called the virtual leader robot and satisfies the nonholonomic constraints, that is, $A(p_d)\dot{p}_d = 0$, the control objective of this paper is to design the voltage control input vector u_{a_i} for ith follower under the following requirements:*

(i) Follower i tracks the virtual leader such that $\lim_{t\to\infty} \left|\rho_i(t) - \rho_i^d(t)\right| < \varepsilon_\rho$ and $\lim_{t\to\infty} \left|\theta_i(t) - \theta_i^d(t)\right| < \varepsilon_\theta$ where $\rho_i(t)$ and $\theta_i(t)$ are the range and relative angle of ith follower with respect to the virtual leader, respectively, which are obtained by sensor measurements. $\rho_i^d(t)$ and $\theta_i^d(t)$ introduce their desired values, respectively, which are commanded by the user (see Fig. 2). The terms ε_ρ and ε_θ are arbitrary small positive constants. Therefore, the tracking error $e_i(t) = z_i(t) - z_d(t) \in \Re^2$ is at least UUB, where $z_d(t) = (x_d, y_d)^T$ and the output vector $z_i(t)$ is defined as follows:

$$z_i(t) = h_i(p_i(t)) = \left(x_i + \rho_i^d \cos\left(\varphi_i + \theta_i^d\right), y_i + \rho_i^d \sin\left(\varphi_i + \theta_i^d\right)\right)^T \tag{9}$$

(ii) The velocity measurements of followers are not available for feedback in real time.
(iii) The robustness of formation controller can be guaranteed in the presence of uncertain dynamics and environmental disturbances.
(iv) The controller design takes the actuator saturation problem into account for all agents to avoid a poor tracking performance in the transient response during formation construction.

Assumption 1. *The reference trajectory is generated by the virtual leader whose motion equations are given by (1) and (6) such that the leader states and derivatives, including p_d, v_d, $\dot{v}_d$ and accordingly $\dot{p}_d$ and $\ddot{p}_d$, are bounded and available signals for all followers.*

Assumption 2. *The desired formation vector $q_i^d = (\rho_i^d, \theta_i^d)^T$ is chosen such that $q_i^d(t)$, $\dot{q}_i^d(t)$, and $\ddot{q}_i^d(t)$ are bounded. Thus, $\sup_{t\geq 0} \|q_i^d(t)\| < \beta_{dpi}$, $\sup_{t\geq 0} \|\dot{q}_i^d(t)\| < \beta_{dvi}$, and $\sup_{t\geq 0} \|\ddot{q}_i^d(t)\| < \beta_{dai}$, where β_{dpi}, β_{dvi}, and β_{dai} are unknown positive constants.*

https://doi.org/10.1017/S026357471900047X Published online by Cambridge University Press

Assumption 3. *The positions and orientations of all followers are measurable in real time. However, their velocity measurements are not available for feedback.*

Remark 1. Since this paper ignores the collision avoidance problem between the followers, the leader is considered to be virtual, and each robot only needs the virtual leader states and its own information; the communication between all robots is not considered in this paper, and our main focus is design of the controller and its stability proof in the next section.

Remark 2. As proved in refs. [31] and [32], the internal dynamics of a WMR is stable in moving forward, but it is unstable when moving backward.

Remark 3. If at least one constraint is nonholonomic, it suggests that the system is not input state linearizable. However, it may be input–output linearizable by choosing a proper set of output equations as (9).[28,33,34]

2.5. WMR formation input–output model

The basic way to obtain an input–output model is differentiating the outputs repeatedly to make an explicit relation with inputs. By differentiating (9) and considering (8), one obtains:

$$\dot{z}_i = L_{f_i}h_i(x_i) + L_{q_i}h_i(x_i) + L_{g_i}h_i(p_i)u_{a_i} + L_{\Delta_i}h_i(p_i) = J_i(p_i)v_i \tag{10}$$

where $L_{f_i}h_i(x_i) = \nabla h_i f_i$, $L_{q_i}h_i(x_i) = \nabla h_i q_i$, $L_{g_i}h_i(x_i) = \nabla h_i g_i$, and $L_{\Delta_i}h_i(x_i) = \nabla h_i \Delta_i$ denote the Lie derivatives of h_i along the direction of the vectors f_i, q_i, g_i, and Δ_i, respectively,[30] and ∇h_i represents the gradient of h_i, $J_i(p_i) = J_{h_i}(p_i)G_i(p_i)$, where $J_{h_i}(p_i) = \partial h_i(p_i)/\partial p_i$ denotes the Jacobian matrix. As is clear from (10), the output is not related to the actuator input. By differentiating again, it yields:

$$\ddot{z}_i = L_{f_i}^2 h_i(x_i) + L_{q_i}L_{f_i}h_i(x_i) + L_{\Delta_i}L_{f_i}h_i(p_i) + L_{g_i}L_{f_i}h_i(p_i)u_{a_i} \tag{11}$$

$$\begin{cases} L_{f_i}^2 h_i(x_i) = \partial(J_{h_i}(p_i)G_i(p_i)v_i)/\partial p_i G_i(p_i)v_i \\ L_{q_i}L_{f_i}h_i(x_i) = -J_{h_i}(p_i)G_i(p_i)\bar{M}_i^{-1}\bar{C}_i(p_i,\dot{p}_i)v_i \\ L_{\Delta_i}L_{f_i}h_i(p_i) = -J_{h_i}(p_i)G_i(p_i)\bar{M}_i^{-1}\left(\bar{F}_i(\dot{p}_i) + \bar{\tau}_{d_i}\right) \\ L_{g_i}L_{f_i}h_i(p_i) = J_{h_i}(p_i)G_i(p_i)K_{1i}\bar{M}_i^{-1}\bar{B}_i \end{cases} \tag{12}$$

where $L_{g_i}L_{f_i}h_i(p_i) := D_i(p_i)$ is introduced as the decoupling matrix. With the assumption $\det(D_i(p_i)) \neq 0$, the systems (8) and (9) are input–output linearizable.

3. Main Results

3.1. Nonlinear control law design and RBF NN approximator structure

In this section, the input voltage vector u_{a_i} is designed as a nonlinear control law for applying to the inner loop feedback as follows:

$$u_{a_i} = \hat{D}_i^{-1}(p_i)\left(\eta_i - L_{f_i}^2 h_i(x_i)\right) \tag{13}$$

where $\eta_i \in \Re^2$ represents the new external input vector. Due to the fact that the decoupling matrix $D_i(p_i)$ includes unknown parameters, it is replaced by its estimation $\hat{D}_i(p_i)$ according to the certainty equivalence principle. By substituting (13) into (11), the following expression is obtained:

$$\ddot{z}_i = \eta_i + L_{q_i}L_{f_i}h_i(x_i) + L_{\Delta_i}L_{f_i}h_i(p_i) + \left(D_i(p_i)\hat{D}_i^{-1}(p_i) - I\right)\left(\eta_i - L_{f_i}^2 h_i(x_i)\right) \tag{14}$$

The RBF NN is used to approximate the terms of nonlinear parametric uncertainties in (14), including the mass, moment of inertia, and actuator parameters,[29] which are employed below for the following nonlinearity:

$$n_i(x_i) = L_{q_i}L_{f_i}h_i(x_i) + \left(D_i(p_i)\hat{D}_i^{-1}(p_i) - I\right)\left(\eta_i - L_{f_i}^2 h_i(x_i)\right) \tag{15}$$

https://doi.org/10.1017/S026357471900047X Published online by Cambridge University Press

Then, there exists an RBF NN with three layers and l nodes for a given continuous function $n_i(x_i)$: $\Re^5 \to \Re^2$ as $\hat{n}_i(x_i|\hat{W}_i) = \hat{W}_i^T \xi_i(x_i)$ such that

$$\hat{W}_i = \begin{pmatrix} \hat{w}_{1,i}^T & 0_{1\times l} \\ 0_{1\times l} & \hat{w}_{2,i}^T \end{pmatrix}^T \tag{16}$$

where $\hat{W}_i$ is the weight matrix, including adjustable parameters $\hat{w}_{k,i} = \left(\hat{w}_{k1,i}, \hat{w}_{k2,i}, \ldots, \hat{w}_{kl,i}\right)^T$, $k = 1, 2$ that can be updated by an adaptive law, which will be defined in the next section; $\xi_i(x_i) = (\xi_{1,i}^T(x_i), \xi_{2,i}^T(x_i))^T$ with $\xi_{k,i}(x_i) = (\xi_{k1,i}(x_i), \xi_{k2,i}(x_i), \ldots, \xi_{kl,i}(x_i))^T$, $k = 1, 2$ is a neural basis function vector, which is fixed *a priori* by the designer:

$$\xi_{kj,i}(x_i) = \exp\left(-\|x_i - \mu_{kj,i}\|^2 / c_{kj,i}^2\right), \quad j = 1, 2, \ldots, l \tag{17}$$

where $\xi_{kj,i}(x_i)$ is jth Gaussian basis function, and $\mu_{kj,i}$ and $c_{kj,i}$ are the center and width of the Gaussian function, respectively. It is considered that x_i and $\hat{W}_i$ belong to compact sets $\Omega_{x_i} \subset \Re^5$ and $\Omega_{W_i} \subset R^l$, respectively. The ideal constant weight vector W_i^* is introduced as:

$$W_i^* = \arg\min_{\hat{W}_i \in \Omega_{W_i}} \left\{ \sup_{x_i \in \Omega_{x_i}} \left| n_i(x_i) - \hat{n}_i(x_i|\hat{W}_i) \right| \right\} \tag{18}$$

Here, $\hat{W}_i$ shows the estimation of W_i^*. The neural estimation error is defined as $\varepsilon_i(x_i) = n_i(x_i) - \hat{n}_i(x_i|W_i^*)$. The nonlinear parametric uncertainty n_i is written as $n_i(x_i) = W_i^{*T} \xi_i(x_i) + \varepsilon_i$. Then, (15) is rewritten as follows:

$$\ddot{z}_i = \eta_i + W_i^{*T} \xi_i(x_i) + \alpha_i^* \tag{19}$$

where $\alpha_i^* = L_{\Delta_i} L_{f_i} h_i(p_i) + \varepsilon_i$ includes nonparametric uncertainties. Assuming that $\|L_{\Delta_i} L_{f_i} h_i(p_i)\| \le \beta_{\Delta_i}$ and $\|\varepsilon_i\| \le \beta_{\varepsilon_i}$, the term α_i^* can be bounded as $\|\alpha_i^*\| \le \alpha_{M_i}^*$, where $\alpha_{M_i}^* = \beta_{\Delta_i} + \beta_{\varepsilon_i}$.

Assumption 4. *The ideal NN weights are bounded such that* $\|\hat{W}_i\| \le W_{M_i}$, *where* W_{M_i} *is an unknown positive constant.*

3.2. High-gain velocity observer design

In real-world applications, the output position vector, including the robot position and heading, can be measured using a global or local sensor. However, the robot velocity vector is difficult to be measured. Therefore, the high-gain observer is employed in this paper to provide the estimation of the velocity vector in the presence of uncertain dynamics and unknown disturbances to implement the output feedback control system.

Lemma 1. **[25, 35]** *Suppose the system output* $z_i(t)$ *and its first* $n-1$ *derivatives are bounded, that is,* $|z_i^{(r)}| < Z_{ri}$, $(r = 0, 1, \ldots, n-1)$ *with positive constants* Z_{ri}. *Consider the following linear system:*

$$\begin{cases} \delta_i \dot{\pi}_{qi} = \pi_{(q+1)i}, \quad q = 1, 2, \ldots, n-1 \\ \delta_i \dot{\pi}_{ni} = -\gamma_{1i}\pi_{ni} - \gamma_{2i}\pi_{(n-1)i} - \cdots - \gamma_{(n-1)i}\pi_{2i} - \pi_{1i} + z_i(t) \end{cases} \tag{20}$$

with δ_i *being a small positive constant, and the parameters* $\gamma_{1i}, \ldots, \gamma_{(n-1)i}$ *are chosen such that the polynomial* $s^n + \gamma_{1i}s^{n-1} + \cdots + \gamma_{(n-1)i}s + 1$ *is Hurwitz. Then, the following properties hold:*

(1) $\pi_{(r+1)i}/\delta_i^r - z_i^{(r)} = -\delta_i \bar{\varphi}_i^{(r+1)}, \quad r = 0, 1, \ldots, n-1$
where $\bar{\varphi}_i = \pi_{ni} + \gamma_{1i}\pi_{(n-1)i} + \cdots + \gamma_{(n-1)i}\pi_{1i}$ *and* $\bar{\varphi}_i^{(r)}$ *denotes the rth derivative of* $\bar{\varphi}_i$.
(2) There exist positive constants t^* *and* β_{ri} *only depending on* $Z_{(r-1)i} (r = 1, 2, \ldots, n)$, δ_i, *and* $\gamma_{qi} (q = 1, \ldots, n-1)$, *such that* $\left|\bar{\varphi}_i^{(r)}\right| \le \beta_{ri}$ *for all* $t > t^*$.

Remark 4. Note that $\pi_{(r+1)i}/\delta_i^r$ asymptotically converges to $z_i^{(r)}$, if z_i and its first rth derivatives are bounded. Hence, $\pi_{(r+1)i}/\delta_i^r$ for $(r = 0, 1, \ldots, n-1)$ is a suitable observation to provide the

https://doi.org/10.1017/S026357471900047X Published online by Cambridge University Press

estimations of the unmeasured output derivatives up to $(n-1)$th order. Moreover, Eq. (20) only depends on the available output signals of the system, and it does not include any information about the mathematical model of the system with unavailable state variables. These advantages cause the high-gain observer to be attractive in the output feedback control design for a class of nonlinear systems with available output, uncertain dynamics, and unknown disturbances.

We can construct the high-gain observer for the formation tracking control of robots as follows:

$$\delta_i \dot{\pi}_{1i} = \pi_{2i}, \tag{21}$$

$$\delta_i \dot{\pi}_{2i} = -\gamma_{1i}\pi_{2i} - \pi_{1i} + z_i(t), \tag{22}$$

where $\pi_{1i}, \pi_{2i} \in \Re^2$ are the state vectors of the high-gain observer. Then, the estimations of $z_i(t)$ and its first derivative $\dot{z}_i(t)$ are presented by:

$$\hat{z}_i = z_i = \pi_{1i}, \quad \dot{\hat{z}}_i = \pi_{2i}/\delta_i \tag{23}$$

According to (10) and (23), the velocity estimation of each mobile robot is obtained by

$$\hat{v}_i = J_i^{-1}(p_i)(\pi_{2i}/\delta_i) \tag{24}$$

Regarding (24) and item 1 of Lemma 1, one achieves:

$$\dot{\hat{z}}_i - \dot{z}_i = \pi_{2i}/\delta_i - \dot{z}_i = -\delta_i \ddot{\bar{\varphi}}_i \tag{25}$$

where $\bar{\varphi}_i = \pi_{2i} + \gamma_{1i}\pi_{1i}$. Furthermore, from (25) and item 2 of Lemma 1, one gains:

$$\left\| \dot{\hat{z}}_i - \dot{z}_i \right\| = \delta_i \left\| \ddot{\bar{\varphi}}_i \right\| \leq \delta_i \beta_{2i} \tag{26}$$

3.3. Proposed controller and stability analysis

In this section, an adaptive robust neural output feedback formation controller is designed based on the high-gain observer. When velocity measurements are available, the following filtered tracking error-like signal $e_{f_i}(t) \in \Re^2$ is defined to design the controller:

$$e_{f_i}(t) = \dot{e}_i(t) + \Lambda_{p_i} Tanh(e_i) \tag{27}$$

The hyperbolic tangent function is used to bound the tracking error variable. This technique helps us reduce the risk of actuator saturation effectively. Then, the following error dynamics is obtained:

$$\dot{e}_{f_i}(t) = \eta_i + W_i^{*^T} \xi_i(x_i) + \alpha_i^* - \ddot{z}_d(t) + \Lambda_{p_i} Sech^2(e_i)\dot{e}_i \tag{28}$$

where α_i^* is defined in (19). Since $\dot{e}_i$ is not available without velocity measurements, the filtered tracking error-like signal, that is, $e_{f_i}(t)$, is replaced by its estimate as follows, by employing (23):

$$\hat{e}_{f_i}(t) = \dot{\hat{e}}_i(t) + \Lambda_{p_i} Tanh(e_i) = \pi_{2i}(t)/\delta_i - \dot{z}_d(t) + \Lambda_{p_i} Tanh(e_i) \tag{29}$$

Then, a neural adaptive robust Proportional Derivative (PD)-like controller is proposed based on the high-gain observer (21) and (22) as follows:

$$\eta_i = \ddot{z}_d(t) - k_{p_i}\hat{e}_{f_i}(t) - \Lambda_{p_i} Sech^2(e_i)\dot{\hat{e}}_i - \hat{W}_i^T \xi_i(\hat{x}_i) - H(\hat{e}_{f_i})\hat{\alpha}_{M_i}, \tag{30}$$

where the elements of $\hat{W}_i$ and $\hat{\alpha}_{M_i}$ are updated by the following adaptive rules:

$$\dot{\hat{w}}_{k,i} = \gamma_{W_{k,i}} \xi_{k,i}(\hat{x}_i)\hat{e}_{f_{k,i}} - \sigma_{W_{k,i}} \gamma_{W_{k,i}} \hat{w}_{k,i}, \tag{31}$$

$$\dot{\hat{\alpha}}_{M_i} = \gamma_{\alpha_i} H_i(\hat{e}_{f_i})\hat{e}_{f_i} - \gamma_{\alpha_i} \Omega_i \left(\hat{\alpha}_{M_i} - \alpha_{M_i}^0\right), \tag{32}$$

where $\gamma_{W_{k,i}} (k = 1, 2)$ and γ_{α_i} denote adaptive gains, $\sigma_{W_{k,i}} (k = 1, 2)$ is a design constant, and $\Omega_i = diag(\omega_{1,i}, \omega_{2,i})$ is a positive definite matrix. $H_i(\hat{e}_{f_i}) = diag(\tanh(\hat{e}_{f_{1,i}}/\varepsilon_{\alpha_{1,i}}), \tanh(\hat{e}_{f_{2,i}}/\varepsilon_{\alpha_{2,i}}))$ where $\varepsilon_{\alpha_{k,i}} > 0 (k = 1, 2)$ is used as a robust term. The design constant vector $\alpha_{M_i}^0 = \left(\alpha_{M_{1,i}}^0, \alpha_{M_{2,i}}^0\right)^T$ is defined with $\alpha_{M_{k,i}}^0 > 0$, $k = 1, 2$. Main results of this paper are summarized by the following theorem:

Main theorem: Consider the motion equations of WMRs, which are given by (1)–(2). Given a bounded continuous desired trajectory, under Assumptions 1–4 and Lemma 1 and Eqs. (13), (16), (21), (22), and (29)–(32), the neural high-gain observer-based controller, derived below,

https://doi.org/10.1017/S026357471900047X Published online by Cambridge University Press

$$
\begin{aligned}
&u_{a_i} = \hat{D}_i^{-1}(p_i)\big(\ddot{z}_d(t) - k_{p_i}\hat{e}_{f_i}(t) - \Lambda_{p_i} Sech^2(e_i)\dot{\hat{e}}_i - \hat{W}_i^T\xi_i(\hat{x}_i) - H(\hat{e}_{f_i})\hat{\alpha}_{M_i} - L_{f_i}^2 h_i(x_i)\big),\\
&\hat{W}_i = \begin{pmatrix} \hat{w}_{1,i}^T & 0_{1\times l} \\ 0_{1\times l} & \hat{w}_{2,i}^T \end{pmatrix}^T, \quad \dot{\hat{w}}_{k,i} = \gamma_{W_{k,i}}\xi_{k,i}(\hat{x}_i)\hat{e}_{f_{k,i}} - \sigma_{W_{k,i}}\gamma_{W_{k,i}}\hat{w}_{k,i},\\
&\dot{\hat{\alpha}}_{M_i} = \gamma_{\alpha_i} H_i(\hat{e}_{f_i})\hat{e}_{f_i} - \gamma_{\alpha_i}\Omega_i\big(\hat{\alpha}_{M_i} - \alpha_{M_i}^0\big),\\
&\hat{e}_{f_i}(t) = \dot{\hat{e}}_i(t) + \Lambda_{p_i} Tanh(e_i), \quad \dot{\hat{e}}_i(t) = \pi_{2i}(t)/\delta_i - \dot{z}_d(t),\\
&\delta_i\dot{\pi}_{1i}(t) = \pi_{2i}(t), \quad \delta_i\dot{\pi}_{2i}(t) = -\gamma_{1i}\pi_{2i}(t) - \pi_{1i}(t) + z_i(t),
\end{aligned}
\tag{33}
$$

ensures that all robots track a desired formation such that tracking and observation errors are UUB and converge to a small ball containing the origin.

Proof. Consider the Lyapunov function $V(t) = \sum_{i=1}^{N} V_i(t)$ for the overall formation system such that

$$
V_i(t) = 0.5 e_{f_i}^T e_{f_i} + \sum_{j=1}^{2} \delta_{p_{j,i}} Ln\cosh(e_{j,i}) + \sum_{k=1}^{2} 0.5\tilde{w}_{k,i}^T\tilde{w}_{k,i}/\gamma_{W_{k,i}} + 0.5\tilde{\alpha}_{M_i}^T\tilde{\alpha}_{M_i}/\gamma_{\alpha_i},
\tag{34}
$$

where $\tilde{\alpha}_{M_i} = \hat{\alpha}_{M_i} - \alpha_{M_i}^*$ and $\tilde{w}_{k,i} = \hat{w}_{k,i} - w_{k,i}^*$ are the parameter and weight estimation errors, respectively. The time derivative of (34) along (27) and (28) leads to:

$$
\begin{aligned}
\dot{V}_i(t) = e_{f_i}^T\big(\eta_i + W_i^{*^T}\xi_i(x_i) + \alpha_i^* - \ddot{z}_d(t) + \Lambda_{p_i} Sech^2(e_i)\dot{e}_i\big) + Tanh^T(e_i)\Lambda_{p_i} e_{f_i}(t)\\
- Tanh^T(e_i)\Lambda_{p_i}^2 Tanh(e_i) + \sum_{k=1}^{2}\tilde{w}_{k,i}^T\dot{\hat{w}}_{k,i}/\gamma_{W_{k,i}} + \tilde{\alpha}_{M_i}^T\dot{\hat{\alpha}}_{M_i}/\gamma_{\alpha_i}
\end{aligned}
\tag{35}
$$

By substituting (30) into (35) and using (31) and (32), one obtains:

$$
\begin{aligned}
\dot{V}_i(t) = &-e_{f_i}^T k_{p_i}\hat{e}_{f_i}(t) - e_{f_i}^T\big(\hat{W}_i^T\xi_i(\hat{x}_i) - W_i^{*^T}\xi_i(x_i)\big) - e_{f_i}^T(H_i(\hat{e}_{f_i})\hat{\alpha}_{M_i} - \alpha_i^*)\\
&- e_{f_i}^T\Lambda_{p_i} Sech^2(e_i)\tilde{e}_{f_i} + Tanh^T(e_i)\Lambda_{p_i} e_{f_i}(t) - Tanh^T(e_i)\Lambda_{p_i}^2 Tanh(e_i)\\
&+ \sum_{k=1}^{2}\tilde{w}_{k,i}^T\xi_{k,i}(\hat{x}_i)\hat{e}_{f_{k,i}} - \sum_{k=1}^{2}\sigma_{w_{k,i}}\tilde{w}_{k,i}^T\hat{w}_{k,i} + \tilde{\alpha}_{M_i}^T\big(H_i(\hat{e}_{f_i})\hat{e}_{f_i} - \Omega_i\big(\hat{\alpha}_{M_i} - \alpha_{M_i}^0\big)\big)
\end{aligned}
\tag{36}
$$

where $\tilde{e}_{f_i}(t) = \hat{e}_{f_i}(t) - e_{f_i}(t) = \dot{\hat{z}}_i(t) - \dot{z}_i(t)$, which is bounded by (26). Regarding the bounded Gaussian function in this paper, it is assumed that $\|\xi_{k,i}(\hat{x}_i)\| \le q_{k,i}$ $(k = 1, 2)$ with constants $q_{k,i} > 0$. Therefore, according to Young's inequality and the property $\xi_{k,i}(\hat{x}_{k,i}) - \xi_{k,i}(x_{k,i}) = \delta_i S_{t_{k,i}}$, where $S_{t_{k,i}}$ is a bounded vector function,[35] one gets:

$$
\begin{aligned}
&-e_{f_i}^T\big(\hat{W}_i^T\xi_i(\hat{x}_i) - W_i^{*^T}\xi_i(x_i)\big) + \sum_{k=1}^{2}\tilde{w}_{k,i}^T\xi_{k,i}(\hat{x}_i)\hat{e}_{f_{k,i}} = -e_{f_i}^T\big(\tilde{W}_i^T + W_i^{*^T}\big)\xi_i(\hat{x}_i)\\
&\quad + e_{f_i}^T W_i^{*^T}\xi_i(x_i) + \hat{e}_{f_i}^T\tilde{W}_i^T\xi_i(\hat{x}_i)\\
&= \tilde{e}_{f_i}^T\tilde{W}_i^T\xi_i(\hat{x}_i) - e_{f_i}^T W_i^{*^T}(-\delta_i S_{t_i}) = \sum_{k=1}^{2}\tilde{w}_{k,i}^T\xi_{k,i}(\hat{x}_i)\tilde{e}_{f_{k,i}} + \sum_{k=1}^{2} w_{k,i}^{*^T}\delta_i S_{t_{k,i}} e_{f_{k,i}}\\
&\le \sum_{k=1}^{2}\big(\|\tilde{w}_{k,i}^T\|\cdot\|\xi_{k,i}(\hat{x}_i)\tilde{e}_{f_{k,i}}\|\big) + \sum_{k=1}^{2} w_{k,i}^{*^T}\delta_i S_{t_{k,i}} e_{f_{k,i}} \le \sum_{k=1}^{2}\Big(\tfrac{\sigma_{w_{k,i}}}{4}\|\tilde{w}_{k,i}\|^2 + \tfrac{q_{k,i}}{\sigma_{w_{k,i}}}\|\tilde{e}_{f_{k,i}}\|^2\Big)\\
&\quad + \sum_{k=1}^{2} w_{k,i}^{*^T}\delta_i S_{t_{k,i}} e_{f_{k,i}}\\
&\le \sum_{k=1}^{2}\tfrac{\sigma_{w_{k,i}}}{4}\|\tilde{w}_{k,i}\|^2 + \tfrac{1}{2}\tilde{e}_{f_i}^T\Lambda_{f_i}\tilde{e}_{f_i} + \tfrac{1}{2}e_{f_i}^T e_{f_i} + \tfrac{1}{2}\sum_{k=1}^{2}\big(\delta_i^2\|S_{t_{k,i}}\|^2\|w_{k,i}^*\|^2\big)
\end{aligned}
\tag{37}
$$

where $\Lambda_{f_i} = diag(2q_{1,i}/\sigma_{w_{1,i}},\ 2q_{2,i}/\sigma_{w_{2,i}})$. By considering (32), one obtains:

$$
\begin{aligned}
&-e_{f_i}^T(H_i(\hat{e}_{f_i})\hat{\alpha}_{M_i} - \alpha_i^*) + \tilde{\alpha}_{M_i}^T\big(H_i(\hat{e}_{f_i})\hat{e}_{f_i} - \Omega_i\big(\hat{\alpha}_{M_i} - \alpha_{M_i}^0\big)\big)\\
&= \sum_{k=1}^{2}\Big(e_{f_{k,i}}\alpha_{M_{k,i}}^* - e_{f_{k,i}}\tanh\Big(\tfrac{\hat{e}_{f_{k,i}}}{\varepsilon_{\alpha_{k,i}}}\Big)\hat{\alpha}_{M_{k,i}} + \hat{e}_{f_{k,i}}\tanh\Big(\tfrac{\hat{e}_{f_{k,i}}}{\varepsilon_{\alpha_{k,i}}}\Big)\tilde{\alpha}_{M_{k,i}}\Big) - \sum_{k=1}^{2}\omega_{k,i}\tilde{\alpha}_{M_{k,i}}\big(\hat{\alpha}_{M_i} - \alpha_{M_i}^0\big)\\
&\le \sum_{k=1}^{2}\Big(|e_{f_{k,i}}|\alpha_{M_{k,i}}^* - e_{f_{k,i}}\tanh\Big(\tfrac{\hat{e}_{f_{k,i}}}{\varepsilon_{\alpha_{k,i}}}\Big)\hat{\alpha}_{M_{k,i}} + \hat{e}_{f_{k,i}}\tanh\Big(\tfrac{\hat{e}_{f_{k,i}}}{\varepsilon_{\alpha_{k,i}}}\Big)\tilde{\alpha}_{M_{k,i}}\Big) - \sum_{k=1}^{2}\omega_{k,i}\tilde{\alpha}_{M_{k,i}}\big(\hat{\alpha}_{M_i} - \alpha_{M_i}^0\big)
\end{aligned}
\tag{38}
$$

https://doi.org/10.1017/S026357471900047X Published online by Cambridge University Press

Considering the following property of the hyperbolic tangent function,[36]

$$0 \le |\chi| - \chi \tanh(\chi/a) \le 0.2785a, \quad \forall a > 0,\ \chi \in \Re \tag{39}$$

and $\left|\tanh(\hat{e}_{f_i}/\varepsilon_{\alpha_i})\right| < 1$, one achieves:

$$\begin{aligned}
&|e_{f_{k,i}}|\alpha^*_{M_{k,i}} - e_{f_i}\tanh\left(\frac{\hat{e}_{f_{k,i}}}{\varepsilon_{\alpha_{k,i}}}\right)\hat{\alpha}_{M_{k,i}} + \hat{e}_{f_{k,i}}\tanh\left(\frac{\hat{e}_{f_{k,i}}}{\varepsilon_{\alpha_{k,i}}}\right)\tilde{\alpha}_{M_{k,i}}\\
&= |\hat{e}_{f_{k,i}} - \tilde{e}_{f_{k,i}}|\alpha^*_{M_{k,i}} + \tilde{e}_{f_{k,i}}\tanh\left(\frac{\hat{e}_{f_{k,i}}}{\varepsilon_{\alpha_{k,i}}}\right)\hat{\alpha}_{M_{k,i}} - \hat{e}_{f_{k,i}}\tanh\left(\frac{\hat{e}_{f_{k,i}}}{\varepsilon_{\alpha_{k,i}}}\right)\alpha^*_{M_{k,i}}\\
&\le |\hat{e}_{f_{k,i}}|\alpha^*_{M_{k,i}} - \hat{e}_{f_{k,i}}\tanh\left(\frac{\hat{e}_{f_{k,i}}}{\varepsilon_{\alpha_{k,i}}}\right)\alpha^*_{M_{k,i}} + |\tilde{e}_{f_{k,i}}|\alpha^*_{M_{k,i}} + \tilde{e}_{f_{k,i}}\tanh\left(\frac{\hat{e}_{f_{k,i}}}{\varepsilon_{\alpha_{k,i}}}\right)\hat{\alpha}_{M_{k,i}}\\
&\le 0.2785\varepsilon_{\alpha_{k,i}}\alpha^*_{M_{k,i}} + |\tilde{e}_{f_{k,i}}|\alpha^*_{M_{k,i}} + \tilde{e}_{f_{k,i}}\tanh\left(\frac{\hat{e}_{f_{k,i}}}{\varepsilon_{\alpha_{k,i}}}\right)\tilde{\alpha}_{M_{k,i}} + \tilde{e}_{f_{k,i}}\tanh\left(\frac{\hat{e}_{f_{k,i}}}{\varepsilon_{\alpha_{k,i}}}\right)\alpha^*_{M_{k,i}}\\
&\le 0.2785\varepsilon_{\alpha_{k,i}}\alpha^*_{M_{k,i}} + \frac{\left|\tilde{e}_{f_{k,i}}\right|^2 + \alpha^{*2}_{M_{k,i}}}{2} + \frac{\left|\tilde{e}_{f_{k,i}}\right|^2 + \tilde{\alpha}^2_{M_{k,i}}}{2} + \frac{\left|\tilde{e}_{f_{k,i}}\right|^2 + \alpha^{*2}_{M_{k,i}}}{2}\\
&= 0.2785\varepsilon_{\alpha_{k,i}}\alpha^*_{M_{k,i}} + \tfrac{3}{2}\left|\tilde{e}_{f_{k,i}}\right|^2 + \alpha^{*2}_{M_{k,i}} + \tfrac{1}{2}\tilde{\alpha}^2_{M_{k,i}}
\end{aligned} \tag{40}$$

Moreover, it is easy to write the following relation:

$$\begin{aligned}
-\omega_{k,i}\tilde{\alpha}_{M_{k,i}}\left(\hat{\alpha}_{M_i} - \alpha^0_{M_i}\right) &= -\tfrac{1}{2}\omega_{k,i}\tilde{\alpha}^2_{M_{k,i}} - \tfrac{1}{2}\omega_{k,i}(\hat{\alpha}_{M_i} - \alpha^0_{M_i})^2 + \tfrac{1}{2}\omega_{k,i}\left(\alpha^*_{M_i} - \alpha^0_{M_i}\right)^2\\
&\le -\tfrac{1}{2}\omega_{k,i}\tilde{\alpha}^2_{M_{k,i}} + \tfrac{1}{2}\omega_{k,i}\left(\alpha^*_{M_i} - \alpha^0_{M_i}\right)^2
\end{aligned} \tag{41}$$

By substituting (40) and (41) into the right-hand side of (38), one obtains:

$$\begin{aligned}
&-e^T_{f_i}(H_i(\hat{e}_{f_i})\hat{\alpha}_{M_i} - \alpha^*_i) + \tilde{\alpha}^T_{M_i}\left(H_i(\hat{e}_{f_i})\hat{e}_{f_i} - \Omega_i\left(\hat{\alpha}_{M_i} - \alpha^0_{M_i}\right)\right)\\
&\le \sum_{k=1}^{2}\left(0.2785\varepsilon_{\alpha_{k,i}}\alpha^*_{M_{k,i}} + \tfrac{3}{2}\left|\tilde{e}_{f_{k,i}}\right|^2 + \alpha^{*2}_{M_{k,i}} + \tfrac{1}{2}\tilde{\alpha}^2_{M_{k,i}}\right) + \sum_{k=1}^{2}\left(-\tfrac{1}{2}\omega_{k,i}\tilde{\alpha}^2_{M_{k,i}} + \tfrac{1}{2}\omega_{k,i}\left(\alpha^*_{M_i} - \alpha^0_{M_i}\right)^2\right)\\
&= 0.2785\Xi^T_i\alpha^*_{M_i} + \tfrac{3}{2}\left|\tilde{e}_{f_i}\right|^2 + \|\alpha^*_{M_i}\|^2 + \tfrac{1}{2}\|\tilde{\alpha}_{M_i}\|^2 - \tfrac{1}{2}\tilde{\alpha}^T_{M_i}\Omega_i\tilde{\alpha}_{M_i} + \tfrac{1}{2}\left(\alpha^*_{M_i} - \alpha^0_{M_i}\right)^T\Omega_i\left(\alpha^*_{M_i} - \alpha^0_{M_i}\right)
\end{aligned} \tag{42}$$

where $\Xi_i = (\varepsilon_{\alpha_{1,i}}, \varepsilon_{\alpha_{2,i}})^T$. By taking the following inequality into account

$$2\tilde{w}^T_{k,i}\hat{w}_{k,i} = \|\tilde{w}_{k,i}\|^2 + \|\hat{w}_{k,i}\|^2 - \|w^*_{k,i}\|^2 \ge \|\tilde{w}_{k,i}\|^2 - \|w^*_{k,i}\|^2, \tag{43}$$

one obtains:

$$-\sum_{k=1}^{2}\sigma_{w_{k,i}}\tilde{w}^T_{k,i}\hat{w}_{k,i} \le \sum_{k=1}^{2}\frac{\sigma_{w_{k,i}}}{2}\|w^*_{k,i}\|^2 - \sum_{k=1}^{2}\frac{\sigma_{w_{k,i}}}{2}\|\tilde{w}_{k,i}\|^2 \tag{44}$$

Considering $\tilde{e}_{f_i}(t) = \dot{\hat{z}}_i - \dot{z}_i$, (26), $\|Sech^2(e_i)\| < 1$, and Young's inequality, we have:

$$\left\|\tilde{e}^T_{f_i}\tilde{e}_{f_i}\right\| = \|\tilde{e}_{f_i}(t)\|^2 = \left\|\dot{\hat{z}}_i - \dot{z}_i\right\|^2 \le \delta^2_i\beta^2_{2i} \tag{45}$$

$$\begin{aligned}
-e^T_{f_i}k_{p_i}\hat{e}_{f_i} = -e^T_{f_i}k_{p_i}(\tilde{e}_{f_i} + e_{f_i}) &\le \tfrac{1}{2}\|e_{f_i}\|^2 + \tfrac{1}{2}\lambda_{\max}\left\{k^T_{p_i}k_{p_i}\right\}\|\tilde{e}_{f_i}\|^2 - e^T_{f_i}k_{p_i}e_{f_i}\\
&\le \tfrac{1}{2}\|e_{f_i}\|^2 + \tfrac{1}{2}\lambda_{\max}\left\{k^T_{p_i}k_{p_i}\right\}\delta^2_i\beta^2_{2i} - \lambda_{\min}\{k_{p_i}\}\|e_{f_i}\|^2
\end{aligned} \tag{46}$$

$$\begin{aligned}
&-e^T_{f_i}\Lambda_{p_i}Sech^2(e_i)\tilde{e}_{f_i}(t) \le \|e_{f_i}\|.\|\Lambda_{p_i}\|.\|Sech^2(e_i)\|.\|\tilde{e}_{f_i}(t)\|\\
&\le \tfrac{1}{2}\lambda_{\max}\{\Lambda_{p_i}\}\|e_{f_i}\|^2 + \tfrac{1}{2}\lambda_{\max}\{\Lambda_{p_i}\}\|\tilde{e}_{f_i}(t)\|^2 \le \tfrac{1}{2}\lambda_{\max}\{\Lambda_{p_i}\}\|e_{f_i}\|^2 + \tfrac{1}{2}\lambda_{\max}\{\Lambda_{p_i}\}\delta^2_i\beta^2_{2i}
\end{aligned} \tag{47}$$

$$Tanh^T(e_i)\Lambda_{p_i}e_{f_i} \le \frac{1}{2}\lambda_{\max}\{\Lambda_{p_i}\}\|Tanh(e_i)\|^2 + \frac{1}{2}\lambda_{\max}\{\Lambda_{p_i}\}\|e_{f_i}\|^2 \tag{48}$$

$$-Tanh^T(e_i)\Lambda^2_{p_i}Tanh(e_i) \le -\lambda_{\min}\{\Lambda^2_{p_i}\}\|Tanh(e_i)\|^2 \tag{49}$$

https://doi.org/10.1017/S026357471900047X Published online by Cambridge University Press

Substituting (37), (42), and (44)–(49) into (36) and changing the arrangement, it yields:

$$\begin{aligned}\dot{V}_i \le & -(\lambda_{\min}\{k_{p_i}-I_2\}-\lambda_{\max}\{\Lambda_{p_i}\})\|e_{f_i}\|^2-(\lambda_{\min}\{\Lambda_{p_i}^2\}-\tfrac{1}{2}\lambda_{\max}\{\Lambda_{p_i}\})\|Tanh(e_i)\|^2\\ & -\min_{i=1,2}\left\{\tfrac{\sigma_{w_{k,i}}}{4}\right\}\|\tilde{w}_{k,i}\|^2-\tfrac{\lambda_{\min}\{\Omega_i\}-1}{2}\|\tilde{\alpha}_{M_i}\|^2+\tfrac{1}{2}\sum_{k=1}^{2}(\delta_i^2\|S_{t_{k,i}}\|^2+\sigma_{w_{k,i}})\|w_{k,i}^*\|^2\\ & +\|\alpha_{M_i}^*\|^2+0.2785\Xi_i^T\alpha_{M_i}^*+\tfrac{1}{2}\left(\alpha_{M_i}^*-\alpha_{M_i}^0\right)^T\Omega_i\left(\alpha_{M_i}^*-\alpha_{M_i}^0\right)\\ & +\tfrac{1}{2}\left(\lambda_{\max}\left\{k_{p_i}^Tk_{p_i}+\Lambda_{f_i}+\Lambda_{p_i}\right\}+3\right)\delta_i^2\beta_{2i}^2\end{aligned} \tag{50}$$

The inequality (50) is re-written as follows:

$$\dot{V}_i(t)\le -c_{m_i}\|x_{t_i}\|^2+\mu_i, \tag{51}$$

where x_{t_i}, c_{m_i}, and μ_i are given by

$$x_{t_i}=\left(e_{f_i}^T,\, Tanh^T(e_i),\, \tilde{w}_{1,i}^T,\, \tilde{w}_{2,i}^T,\, \tilde{\alpha}_{M_i}\right)^T \tag{52}$$

$$c_{m_i}=\min\left\{\lambda_{\min}\{k_{p_i}-I_2\}-\lambda_{\max}\{\Lambda_{p_i}\},\, \lambda_{\min}\left\{\Lambda_{p_i}^2\right\}-\frac{1}{2}\lambda_{\max}\left\{\Lambda_{p_i}\right\},\, \min_{i=1,2}\left\{\frac{\sigma_{w_{k,i}}}{4}\right\},\, \frac{\lambda_{\min}\{\Omega_i\}-1}{2}\right\} \tag{53}$$

$$\begin{aligned}\mu_i=&\tfrac{1}{2}\textstyle\sum_{k=1}^{2}(\delta_i^2\|S_{t_{k,i}}\|^2+\sigma_{w_{k,i}})\|w_{k,i}^*\|^2+\|\alpha_{M_i}^*\|^2+0.2785\Xi_i^T\alpha_{M_i}^*\\ &+\tfrac{1}{2}\left(\alpha_{M_i}^*-\alpha_{M_i}^0\right)^T\Omega_i\left(\alpha_{M_i}^*-\alpha_{M_i}^0\right)+\tfrac{1}{2}\left(\lambda_{\max}\left\{k_{p_i}^Tk_{p_i}+\Lambda_{f_i}+\Lambda_{p_i}\right\}+3\right)\delta_i^2\beta_{2i}^2\end{aligned} \tag{54}$$

Regarding (53), the design matrices k_{p_i} and Ω_i should satisfy:

$$\lambda_{\min}\{k_{p_i}-I_2\}>\lambda_{\max}\{\Lambda_{p_i}\}\ ,\ \lambda_{\min}\left\{\Lambda_{p_i}^2\right\}>0.5\lambda_{\max}\{\Lambda_{p_i}\}\ \ ,\ \ \lambda_{\min}\{\Omega_i\}>1 \tag{55}$$

Then, inequality (53) can be expressed as follows for the overall formation system:

$$\dot{V}(t)\le\sum_{i=1}^{N}(-c_{m_i}\|x_{t_i}(t)\|^2+\mu_i)\le -c_{\min}\|x_t(t)\|^2+\mu, \tag{56}$$

where $x_t(t)=(x_{t_1}^T,x_{t_2}^T,\ldots,x_{t_N}^T)^T$, $c_{\min}=\min\{c_{m_i}\}\big|_{i=1}^N$, and $\mu=\sum_{i=1}^N\mu_i$. Thus, if the condition (55) is satisfied, $\dot{V}(t)$ is strictly negative outside the compact set $\Omega_{x_t}=\{x_t(t)|\,0\le\|x_t(t)\|\le\sqrt{\mu/c_{\min}}\}$, which means that $V(t)$ is decreasing outside the set Ω_{x_t}. It proves $\|x_t(t)\|$ is UUB, which implies that tracking and observation errors, NN weights, and parameter estimation errors exponentially converge to a small ball containing origin. This completes the proof.

3.4. Discussion on controller gain tuning

It is clear from (53) and (54) that $\sqrt{\mu/c_{\min}}$ can be provided as small as required by appropriately choosing the positive definite design matrices k_{p_i}, Λ_{p_i}, and Ω_i, and positive design constants δ_i, $\gamma_{W_{k,i}}$, $\sigma_{w_{k,i}}$, γ_{α_i}, and $\varepsilon_{\alpha_{k,i}}$ ($k=1,2$), satisfying (55). One may use the following tuning rules to adjust control parameters properly: (*i*) the inverse relationship between the size of ultimate bound $\mu/c_{\min}$ and gain Λ_{p_i} can be seen from (53), as c_{m_i} tends to increase with $\lambda_{\min}\{\Lambda_{p_i}^2\}-0.5\lambda_{\max}\{\Lambda_{pi}\}$. We do not, however, see the same analytical relationship for k_{p_i}, as μ_i depends on k_{p_i}. Therefore, the larger value of Λ_{p_i} and smaller value of δ_i decrease μ_i, which reduces the size of ultimate bound $\mu/c_{\min}$ and improves convergence rate and final tracking accuracy; (*ii*) the large values of adaptive gains, that is, $\gamma_{W_{k,i}}$ and γ_{α_i} in (31) and (32), lead to a better final tracking accuracy. However, a larger adaptive gain γ_{α_i} may cause more robust control actions, which generate control signal chattering; (*iii*) smaller values of $\sigma_{w_{k,i}}$ and Ω_i decrease the value of μ_i in (54), which leads to a smaller ultimate bound $\mu/c_{\min}$ and better final tracking accuracy. However, decreasing $\sigma_{w_{k,i}}$ and Ω_i may lower robustness of parameter update rules in (31) and (32); (*iv*) one may compromise between final tracking accuracy and smoothness of control signals by tuning of the boundary layer thickness $\varepsilon_{\alpha_{k,i}}$. The proposed

https://doi.org/10.1017/S026357471900047X Published online by Cambridge University Press

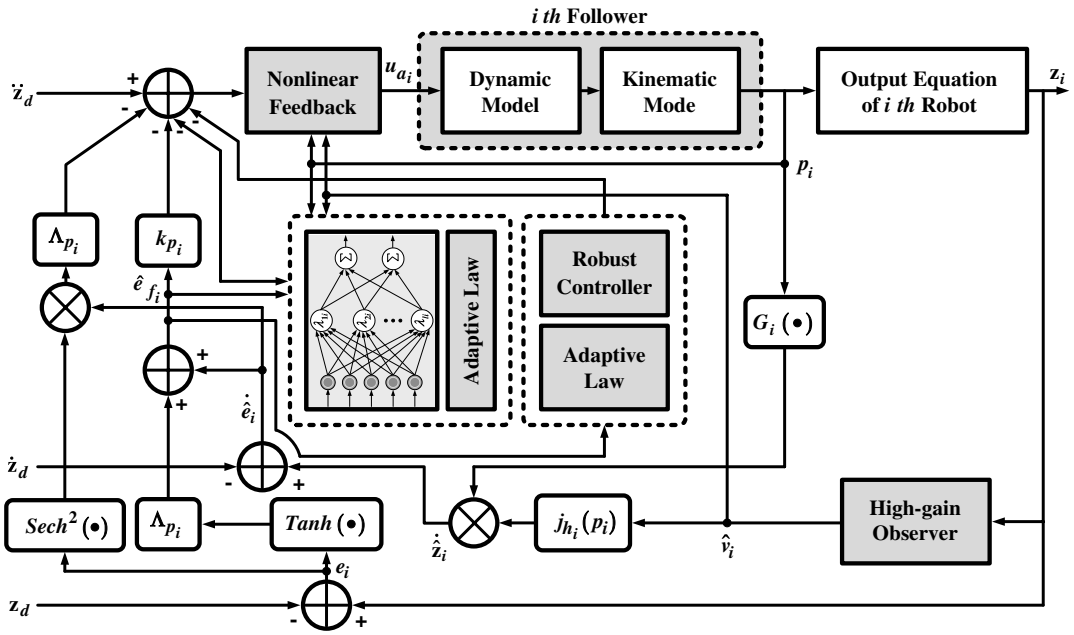

Fig. 3. A block diagram of the proposed NN control system.

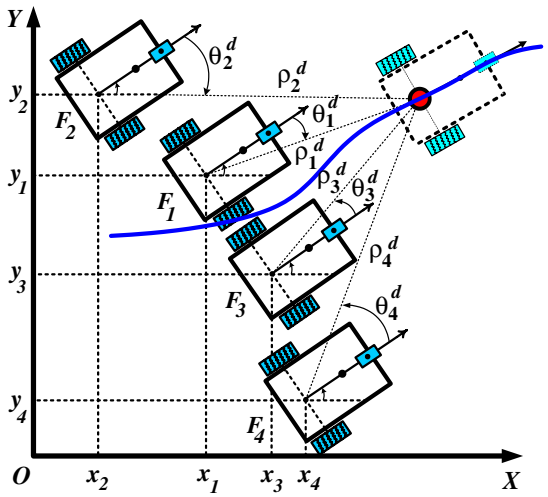

Fig. 4. The desired leader–follower formation configuration.

controller can be made smoother, and it prevents actuator chattering and saturation by selecting larger values for $\varepsilon_{\alpha_{k,i}}$. However, larger values of $\varepsilon_{\alpha_{k,i}}$ increases the value of μ_i in (54), which may result in a larger ultimate bound $\mu/c_{\min}$ and decrease final tracking accuracy. It should be mentioned that the control parameters will be adjusted by a trial-and-error method based on the proposed gain-tuning rules. Figure 3 demonstrates a block diagram of the proposed output feedback formation controller.

4. Numerical Examples

4.1. Simulation results

In this section, some computer simulations are performed to demonstrate the effectiveness and efficiency of the proposed formation controller for a group of four identical WMRs based on the high-gain observer with saturating actuators. All the simulations are performed in MATLAB software in a computer whose processor is an Intel Core i7 with 2 GHz frequency and 6 GB RAM. Simulations are carried out based on Euler approximation with a sampling time of 20 ms. By adding

https://doi.org/10.1017/S026357471900047X Published online by Cambridge University Press

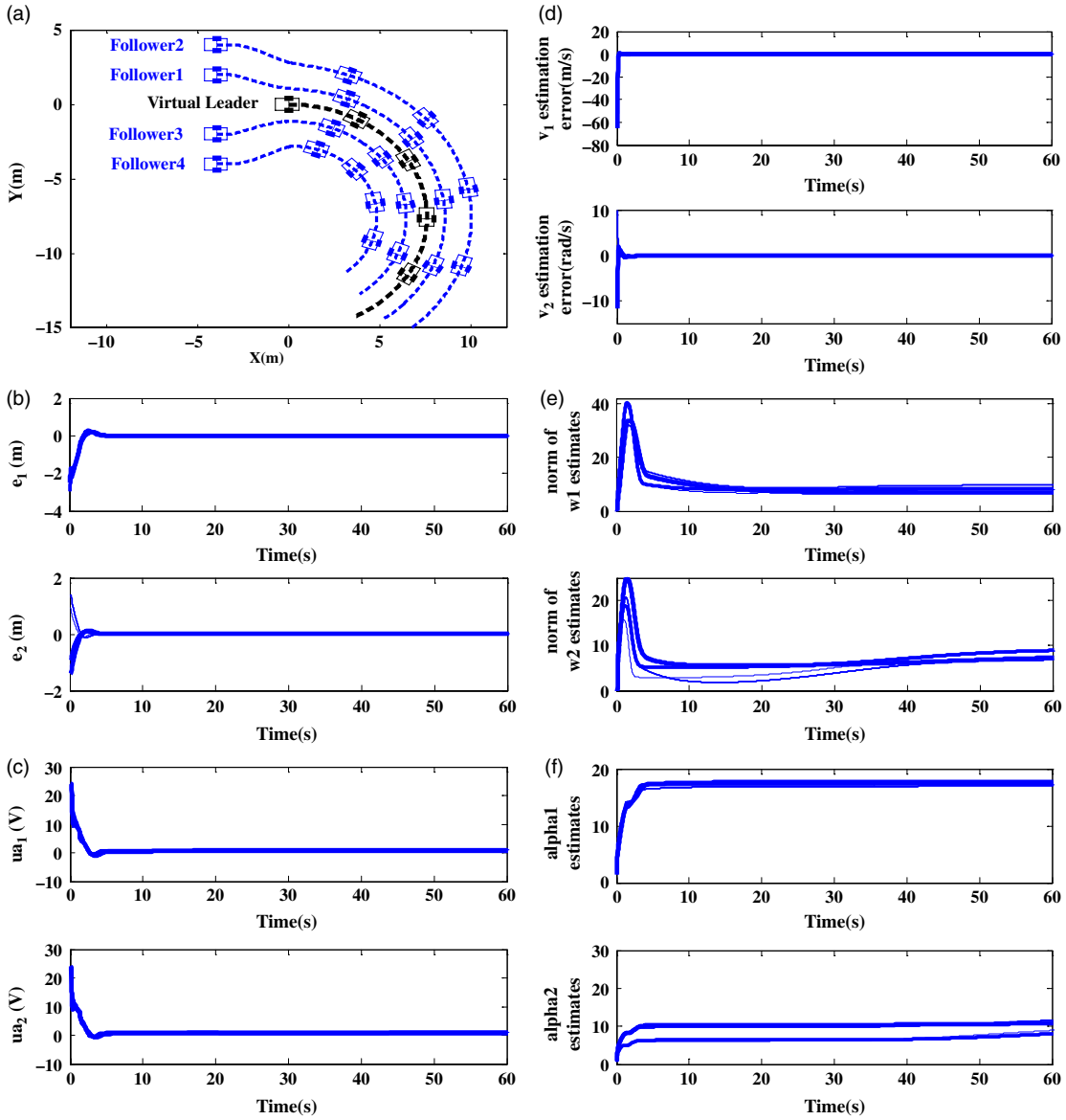

Fig. 5. Simulation results of circle trajectory formation tracking: (a) *x*–*y* plot, (b) tracking errors, (c) control signals, (d) velocity estimation errors, (e) norm of weight estimates, and (f) alpha estimates.

a zero-mean Gaussian white noise to the measured signals, including positions and orientation using *randn*(•) function, real sensors are simulated. The standard deviations of the robot positions and orientation noise are selected as 0.003 m and 0.005 rad, respectively, for this simulation. It is also assumed that the robots employ a similar localization system.[37,38] It is supposed that the slippages of robot wheels are insignificant for simplicity in this paper.

To simulate nonparametric uncertainties such as friction, unmodeled dynamics, and environmental disturbances, the following models are chosen:

$$F_i(\dot{p}_i) = 0.5(v_{1,i},\, v_{2,i})^T + 0.8(sgn(v_{1,i}),\, sgn(v_{2,i}))^T \tag{57}$$

$$\tau_{d_i} = 2(\sin(0.05t),\, \sin(0.05t))^T \tag{58}$$

The physical parameters of each mobile robot are chosen as $b_i = 0.4\,\text{m}$, $d_i = 0.1\,\text{m}$, $m_{ci} = 10\,\text{kg}$, $m_{wi} = 0.5\,\text{kg}$, $I_{ci} = 3\,\text{kg}\cdot\text{m}^2$, $I_{mi} = 0.006\,\text{kg}\cdot\text{m}^2$, and $r_i = 0.25\,\text{m}$. In order to evaluate the robustness of the proposed controller, it is assumed that all of the model parameters are unknown. The parameters for actuator dynamics are chosen as $n_i = 62.55$, $R_{a_i} = 1.6\,\Omega$, $L_{a_i} = 0.48$

https://doi.org/10.1017/S026357471900047X Published online by Cambridge University Press

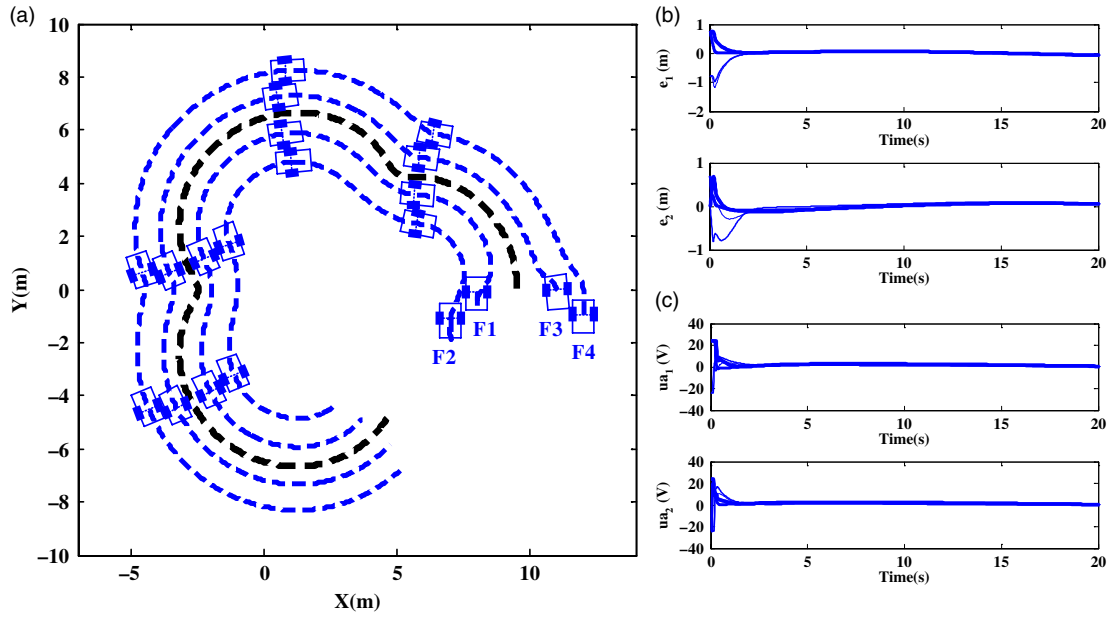

Fig. 6. Simulation results of the controller: (a) x–y plot, (b) tracking errors, and (c) control signals.

Ωs, $K_{bi} = 0.019\,\mathrm{V}/\mathrm{rad}/\mathrm{s}$, and $K_{\tau_i} = 0.2639\,oz - \mathrm{in}/\mathrm{A}$. The controller gains are adopted as $\delta_i = 0.04$, $\gamma_{1i} = 2$, $k_{p_i} = 10I_2$, $\Lambda_{p_i} = 5I_2$, $\gamma_{\alpha_i} = 2$, $\omega_{1,i} = 10^{-5}$, $\omega_{2,i} = 10^{-15}$, $\varepsilon_{\alpha_{1,i}} = 0.08$, and $\varepsilon_{\alpha_{2,i}} = 0.075$. In addition, a three-layer NN with 13 hidden nodes, 2 output nodes, and the parameters $\gamma_{W_{1,i}} = 10$, $\gamma_{W_{2,i}} = 15$, $\sigma_{w_{1,i}} = \sigma_{w_{2,i}} = 10^{-5}$, $c_{k,i} = 5(1, 1, 1, 1, 1, 1, 1, 1, 1, 1, 1, 1, 1)^T (k = 1, 2)$, $\mu_{k,i} = (-6, -5, -4, -3, -2, -1, 0, 1, 2, 3, 4, 5, 6)^T (k = 1, 2)$ are designed for the control system. The initial conditions $\alpha^0_{M_i} = 0_{2\times 1}$, $\hat{w}_{1,i}(0) = 0_{l\times 1}$, $\hat{w}_{2,i}(0) = 0_{l\times 1}$, $\pi_{1i}(0) = 0_{2\times 1}$, $\pi_{2i}(0) = 0_{2\times 1}$ are considered. Moreover, the velocities of all followers are initially set to zero. The planar configuration of the desired formation of the followers with respect to the leader is shown by Fig. 4. In this figure, four followers are denoted by F_i, $i = 1, 2, 3, 4$. The desired formation vectors are chosen as $q^d_1(t) = (1.5\mathrm{m}, -45°)^T$, $q^d_2(t) = (3\mathrm{m}, -60°)^T$, $q^d_3(t) = (1.5\mathrm{m}, 45°)^T$, and $q^d_4(t) = (3\mathrm{m}, 60°)^T$.

Three simulation scenarios are carried out based on the mentioned controller settings to demonstrate the effectiveness of the proposed formation controller.

Scenario 1: The open-loop control command for the virtual leader vehicle, which generates the circle trajectory, is set to $u_{a_d} = (0.9\mathrm{V}, 1\mathrm{V})^T$. The initial positions and orientations of all followers and the virtual leader are represented as $p_1(0) = (-4\,\mathrm{m}, 2\,\mathrm{m}, 0\,\mathrm{rad})^T$, $p_2(0) = (-4\,\mathrm{m}, 4\mathrm{m}, 0\mathrm{rad})^T$, $p_3(0) = (-4\,\mathrm{m}, -2\,\mathrm{m}, 0\,\mathrm{rad})^T$, $p_4(0) = (-4\,\mathrm{m}, -4\,\mathrm{m}, 0\,\mathrm{rad})^T$, and $p_d(0) = (0\mathrm{m}, 0\,\mathrm{m}, 0\,\mathrm{rad})^T$, respectively. The simulation results are plotted in Fig. 5(a)–(f). As shown in Fig. 5(a), all followers nicely track their reference trajectory with a satisfactory performance, despite time-varying disturbance. Figure 5(b) shows that output values $z_{1,i}$ and $z_{2,i}$ arrive at the desired target value $z_d = (0\mathrm{m}, 0\,\mathrm{m})^T$ in 2 s. As depicted by Fig. 5(c), the control signals remain within $|u_{a_i}| \le 24\mathrm{V}$, which we have set as the saturation limit. It is clear from Fig. 5(d) that the high-gain observer estimates converge to the output derivatives. The estimates peak at their relative saturation values in 0.8 s, and then converge to the actual output derivatives. As seen in Fig. 5(e), the norms of approximation weights are bounded. The estimated parameters of the upper bound for nonparametric uncertainty are shown by Fig. 5(f).

Scenario 2: The following desired trajectory $z_d(t) = (x_d, y_d)^T$ is chosen to evaluate controller performance:

$$\begin{cases} x_d = x_g + R_0 \cos(\omega_0 t) + R_1 \cos(4\omega_0 t), \\ y_d = y_g + R_0 \sin(\omega_0 t) + R_1 \sin(4\omega_0 t), \end{cases} \tag{59}$$

where $x_g = 2.5$, $y_g = 0$, $R_0 = 6$, $R_1 = 1$, and $\omega_0 = 0.05$. The initial postures of followers are set as $p_1(0) = (8\,\mathrm{m}, 0\,\mathrm{m}, \pi/2\,\mathrm{rad})^T$, $p_2(0) = (7\,\mathrm{m}, -1\mathrm{m}, \pi/2\mathrm{rad})^T$, $p_3(0) = (11\,\mathrm{m}, 0\,\mathrm{m}, \pi/2\,\mathrm{rad})^T$, and$p_4(0) = (12\mathrm{m}, -1\,\mathrm{m}, \pi/2\,\mathrm{rad})^T$. As shown in Fig. 6(a)–(c), the proposed controller successfully

https://doi.org/10.1017/S026357471900047X Published online by Cambridge University Press

Table II. Quantitative comparison of the controller in ref. [26] and the proposed controller.

	Controller in ref. [26]			Proposed controller		
Performance index	**Scenario 1**	**Scenario 2**	**Scenario 3**	**Scenario 1**	**Scenario 2**	**Scenario 3**
$rms(e_{1,i}(t))\ (m)$	0.2073	0.3268	5.6391	0.1945	0.1888	3.0595
$rms(e_{2,i}(t))\ (m)$	0.0645	0.0674	3.2101	0.0403	0.1945	1.5396
$rms(u_{a_{1,i}}(t))\ (V)$	3.4137	4.8544	24.8865	1.9691	4.4967	14.7200
$rms(u_{a_{2,i}}(t))\ (V)$	4.3274	10.8286	49.2354	2.3261	8.6882	15.8506

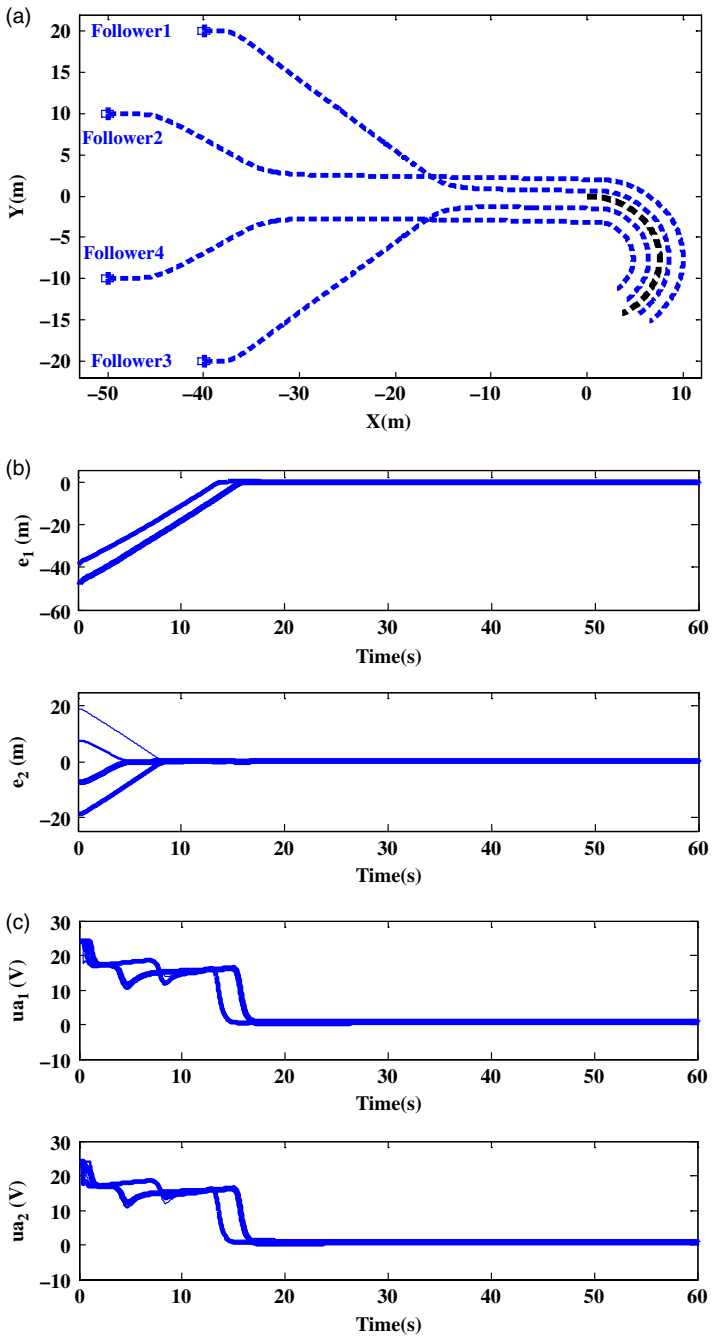

Fig. 7. Simulation results of the proposed controller for large initial tracking errors: (a) *x*–*y* plot, (b) tracking errors, and (c) control signals.

https://doi.org/10.1017/S026357471900047X Published online by Cambridge University Press

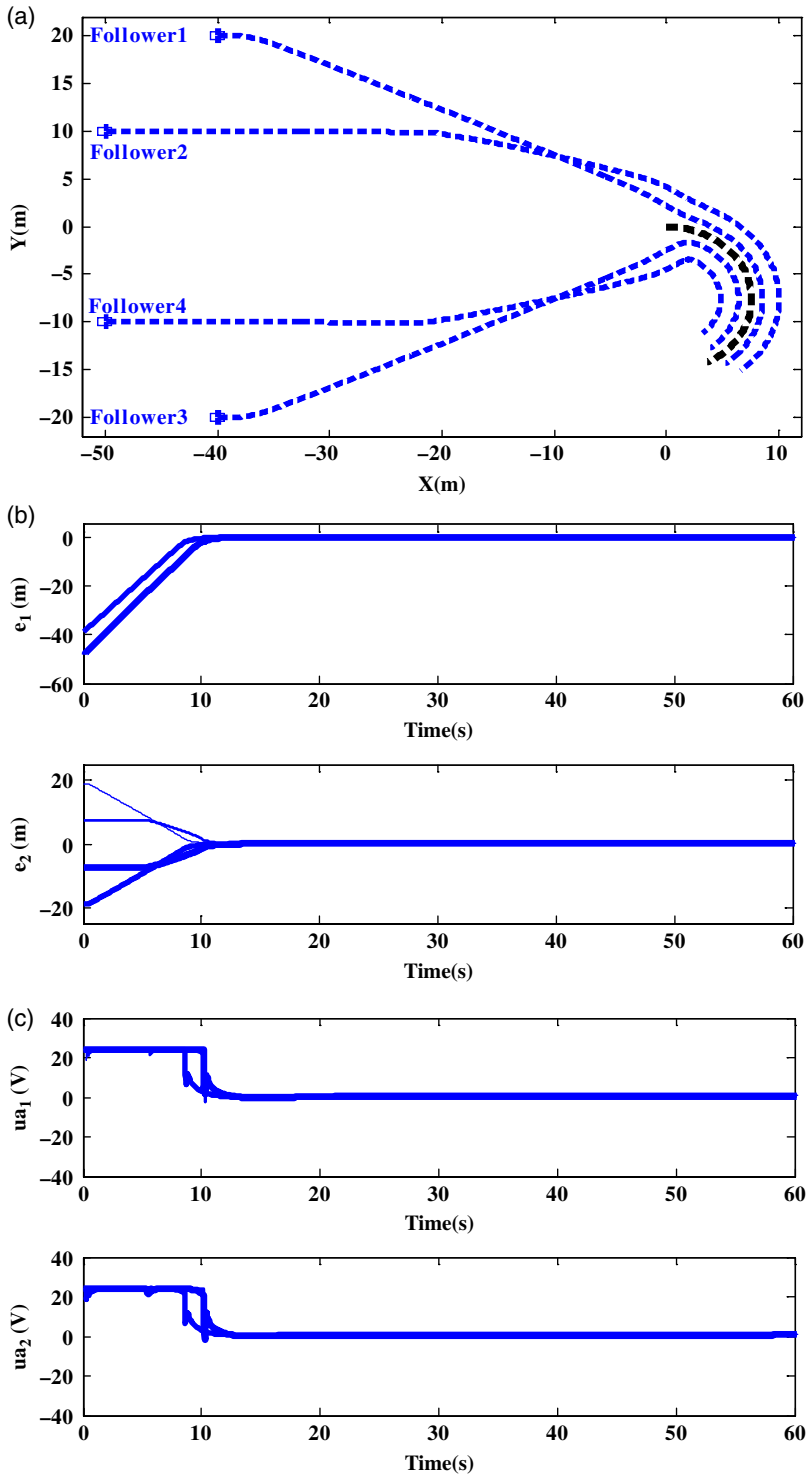

Fig. 8. Simulation results of the controller in [26] for large initial tracking errors: (a) *x*–*y* plot, (b) tracking errors, and (c) control signals.

copes with the trajectory tracking problem in the presence of model uncertainties, environmental disturbances, actuator constraints, and only position measurements.

Scenario 3: It is proven that the proposed controller meets all of the determined control objectives. Therefore, this scenario is carried out for very large initial tracking errors to evaluate the capability of the proposed formation controller in the presence of actuator saturation. Besides, it is of interest to compare this controller with the designed controller in ref. [26]

https://doi.org/10.1017/S026357471900047X Published online by Cambridge University Press

from both qualitative and quantitative aspects. The initial postures of all followers are given by $p_1(0) = (-40\,\text{m}, 20\,\text{m}, 0\,\text{rad})^T$, $p_2(0) = (-50\,\text{m}, 10\,\text{m}, 0\text{rad})^T$, $p_3(0) = (-40\,\text{m}, -20\,\text{m}, 0\,\text{rad})^T$, and $p_4(0) = (-50\text{m}, -10\,\text{m}, 0\text{rad})^T$. The simulation results are depicted in Fig. 7(a)–(c). It is clear that the formation tracking mission is successful and actuator saturation is effectively prevented in spite of the large initial postures of the vehicles, while the amplitudes of control signals remain in $|u_{a_i}| \leq 24\text{V}$. Moreover, tracking errors smoothly converge to a small bound containing the origin.

4.2. A comparative study

In order to evaluate the effectiveness of the proposed controller, a controller similar to that used in Du *et al.*[26] is considered with the same presented adaptive laws as in (31) and (32):

$$u_{a_i} = -J_i^{-1}(p_i)z_{1i} - K_{2i}\hat{z}_{2i} + \hat{W}_i^T\xi_i(\hat{x}_i) - H_i(\hat{z}_{2i})\hat{\alpha}_{M_i} \tag{60}$$

where $z_{1i} = z_i - z_d$ and $z_{2i} = v_i - \alpha_{1i}$ are the outer and inner loop tracking errors, respectively. The intermediate control function vector α_{1i} for the virtual control vector v_i is selected as:

$$\alpha_{1i} = -J_i^{-1}(p_i)K_{1i}z_{1i} \tag{61}$$

The parameters of the controller are chosen as $K_{1i} = 2$, $K_{2i} = 10$, $\delta_i = 0.2$, $\gamma_{1i} = 2$,$\gamma_{\alpha_i} = 10$, $\omega_{1,i} = 10^{-5}$, $\omega_{2,i} = 10^{-15}$, $\varepsilon_{\alpha_{1,i}} = 5$, and $\varepsilon_{\alpha_{2,i}} = 2$. The NN gains are chosen similar to previous values for the proposed controller in this paper. The initial conditions are set to zero. The simulation results for very large initial tracking errors are provided by Fig. 8(a)–(c). As can be seen from comparing the results of simulations, the proposed controller in this paper provides a smoother transient response than the controller (60). In contrast, the controller (60) causes actuator saturation and its control signals are not smoother than the proposed controller signals in this paper.

The following performance indexes are introduced as in refs. [39] and [40] for a fair comparative study of the controllers in terms of quantity:

- The following root mean square of the tracking error is defined to evaluate the *average tracking performance*:

$$rms(e_{j,i}(t)) = \sqrt{(1/T_f)\int_0^{T_f} |e_{j,i}(t)|^2\, dt}, \quad j = 1, 2 \tag{62}$$

  where T_f denotes the total running time and $e_{j,i}$ represents the tracking error for jth output.
- In order to measure the amount of control power consumption, the following *rms* of the control signals is used to evaluate the amount of control efforts:

$$rms(u_{a_{j,i}}(t)) = \sqrt{(1/T_f)\int_0^{T_f} |u_{a_{j,i}}(t)|^2\, dt} \qquad j = 1, 2 \tag{63}$$

Table II shows the numerical values of the above performance indexes, which compare the controllers from the viewpoint of average tracking performance and power consumption. It clearly shows that the amount of control efforts for our proposed controller is smaller than that of the controller in ref. [26]. A main conclusion from Table II is that the proposed controller is more effective than the controller in ref. [26], especially for large initial tracking errors considering the actuator saturation.

5. Conclusion

In this paper, a NN-based leader–follower formation tracking control problem of nonholonomic mobile robots is studied in the presence of actuator saturation and without velocity measurements. The proposed control scheme only relies on the position and heading measurements of robots, and the high-gain observer is designed to estimate unavailable velocities of all robots. In order to reduce the risk of actuator saturation, hyperbolic tangent saturation functions are applied effectively to design a formation controller that generates small-amplitude voltage input signals. Consequently, the transient performance of the proposed controller is improved for large initial tracking errors. Moreover, the proposed controller can efficiently compensate both parametric and nonparametric uncertainties without the requirement of *a prior* knowledge of the robot's dynamics and environmental

https://doi.org/10.1017/S026357471900047X Published online by Cambridge University Press

disturbances via an effective combination of RBF NNs and adaptive robust techniques. A Lyapunov-based stability analysis is presented to guarantee UUB of formation tracking and observation errors. Simulation results indicated the effectiveness of the proposed formation control scheme.

References

1. T. Balch and R. C. Arkin, "Behavior-based formation control for multirobot teams," *IEEE Trans. Rob. Autom.* **14**(6), 926–939 (1998).
2. J. Fredslund and M. J. Mataric, "A general algorithm for robot formations using local sensing and minimal communication," *IEEE Trans. Rob. Autom.* **18**(5), 837–846 (2002).
3. C. B. Low, "A flexible virtual structure formation keeping control design for nonholonomic mobile robots with low-level control systems, with experiments," **In**: *IEEE International Symposium on Intelligent Control*, Juan Les Pins, France (2014) pp. 1576–1582.
4. M. A. Lewis and K.-H. Tan, "High precision formation control of mobile robots using virtual structures," *Auton. Rob.* **4**(4), 387–403 (1997).
5. B. S. Park and S. J. Yoo, "Adaptive leader-follower formation control of mobile robots with unknown skidding and slipping effects," *Int. J. Control, Autom. Syst.* **13**(3), 587–594 (2015).
6. K. Shojaei, "Neural network formation control of underactuated autonomous underwater vehicles with saturating actuators," *Neurocomputing* **194**, 372–384 (2016).
7. J. P. Desai, J. Ostrowski and V. Kumar, "Controlling formations of multiple mobile robots," **In**: *IEEE International Conference Robotics and Automation*, vol. 4 (IEEE, Leuven, 1998) pp. 2864–2869.
8. N. A. Martins, E. S. Youssef, D. W. Bertol, D. E. Pieri, U. F. Moreno and E. B. Castelan, "Trajectory tracking of a nonholonomic mobile robot with kinematic disturbances a variable structure control design," *IEEE Latin Am Trans.* **9**(3), 276–283 (2011).
9. J. Chen, D. Sun, J. Yang and H. Y. Chen, "Leader-follower formation control of multiple non-holonomic mobile robots incorporating Receding-Horizon scheme," *Int. J. Rob. Res.* **29**(6), 727–747 (2009).
10. Y. H. Chang, C. W. Chang, C. L. Chen and C. W. Tao, "Fuzzy sliding-mode formation control for multirobot systems: Design and implementation," *IEEE Trans. Syst. Man Cybern.* **42**, 444–457 (2012).
11. Z. Peng, G. Wen, A. Rahmani and Y. Yu, "Leader-follower formation control of nonholonomic mobile robots based on a bioinspired neurodynamic based approach," *Rob. Auton. Syst.* **61**(9), 988–996 (2013).
12. T. Dierks, B. Brenner and S. Jagannathan, "Neural network-based optimal control of mobile robot formations with reduced information exchange," *IEEE Trans. Control Syst. Technol.* **21**(4), 1407–1415 (2013).
13. A. Guillet, R. Lenain, B. Thuilot and P. Martinet, "Adaptable robot formation control: Adaptive and predictive formation control of autonomous vehicles," *IEEE Rob. Autom. Mag.* **21**, 28–39 (2014).
14. K. Shojaei, A. M. Shahri and B. Tabibian, "Design and implementation of an inverse dynamics controller for uncertain nonholonomic robotic systems," *J. Intell. Rob. Syst.* **71**(1), 65–83 (2013).
15. K. D. Do and J. Pan, "Global output-feedback path tracking of unicycle-type mobile robots," *Rob. Comput.-Integr. Manufact.* **22**, 166–179 (2006).
16. T. Sun, F. Liu, H. Pei and Y. He, "Observer-Based adaptive leader-following formation control for non-holonomic mobile robots," *IET Control Theory Appl.* **6**(18), 2835–2841 (2012).
17. B. S, Park, S. J. Yoo, J. B. Park and Y. H. Choi, "Adaptive output-feedback control for trajectory tracking of electrically driven non-holonomic mobile robots," *IET Control Theory Appl.* **5**(6), 830–838 (2011).
18. K. Shojaei and A. M. Shahri, "Output feedback tracking control of uncertain nonholonomic wheeled mobile robots: A dynamic surface control approach," *IET Control Theory Appl.* **6**(2), 216–228 (2012).
19. K. Shojaei, "Observer-based neural adaptive formation control of autonomous surface vessels with limited torque," *Rob. Auton. Syst.* **78**, 83–96 (2016).
20. Y. Cheng, R. Jia, H. Du, G. Wen and W. Zhu, "Robust finite-time consensus formation control for multiple nonholonomic wheeled mobile robots via output feedback," *Int. J. Robust Nonlinear Control* **28**(6), 2082–2096 (2017).
21. M. Hassan, E. Aljuwaiser and R. Badr, "A new on-line observer-based controller for leader-follower formation of multiple nonholonomic mobile robots," *J. Franklin Institute* **355**(5), 2436–2472 (2018).
22. J. Yu, X. Dong, Q. Li and Z. Ren, "Practical time-varying formation tracking for multiple non-holonomic mobile robot systems based on the distributed extended state observers," *IET Control Theory Appl.* **12**(12), 1737–1747 (2018).
23. K. Shojaei, "Neural adaptive PID formation control of car-like mobile robots without velocity measurements," *Adv. Rob.* **31**(18), 947–964 (2017).
24. F. Esfandiari and H. K. Khalil, "Observer-based design of uncertain systems: Recovering state feedback robustness under matching conditions," **In**: *Proceedings of Allerton Annual Conference on Communication, Control and Computing*, University of Illinois, Monticello, IL, USA (1987) pp. 97–106.
25. K. P. Tee and S. S. Ge, "Control of fully actuated ocean surface vessels using a class of feedforward approximators," *IEEE Tran. Control Syst. Technol.* **14**, 750–756 (2006).
26. J. Du, X. Hu, H. Liu and C. L. P. Chen, "Adaptive robust output feedback control for marine dynamic positioning system based on a high-gain observer," *IEEE Trans. Neural Networks Learn. Syst.* **26**, 2775–2786 (2015).

https://doi.org/10.1017/S026357471900047X Published online by Cambridge University Press

27. S. G. Tzafestas, *Introduction to Mobile Robot Control*, 1st Edition (Elsevier, New York, USA, 2014).
28. N. Sarkar, X. Yun and V. Kumar, "Control of mechanical systems with rolling constraints application to dynamic control of mobile robots," *Int. J. Rob. Res.* **13**(1), 55–69 (1994).
29. F. L. Lewis, D. M. Dawson and C. T. Abdallah, *Robot Manipulator Control Theory and Practice*. 2nd ed. Revised and Expanded (Marcel Dekker, New York, USA, 2004).
30. H. Khalil, *Nonlinear Systems*, Third Edition (Prentice Hall, Englewood Cliffs, NJ, USA, 2002).
31. X. Yun and Y. Yamamoto, "Stability analysis of the internal dynamics of a wheeled mobile robot," *J. Rob. Syst*. **14**(10), 697–709 (1997).
32. D. Wang and G. Xu, "Full-state tracking and internal dynamics of nonholonomic wheeled mobile robots," *IEEE/ASME Trans. Mechatron*. **8**(2), 203–214 (2003).
33. Y. Yamamoto, Control and coordination of locomotion and manipulation of wheeled mobile manipulators *Ph.D. Thesis* (University of Pennsylvania, PA, USA, 1994).
34. K. Shojaei, A. Tarakameh and A. M. Shahri, "Adaptive trajectory tracking of WMRs based on feedback linearization technique," **In**: *Proceedings of 2009 IEEE International Conference on Mechatronics and Automation* (IEEE, Changchun, China, 2009) pp. 729–734.
35. S. S. Ge, C. C. Hang, T. H. Lee, and T. Zhang, *Stable Adaptive Neural Network Control* (Kluwer Academic, Boston, MA, USA, 2001).
36. M. M. Polycarpou and P. A. Ioannou "Stable adaptive neural control scheme for nonlinear systems," *IEEE Trans. Autom. Control* **41**(3), 447–451 (1996).
37. K. Shojaei and A. M. Shahri, "Experimental study of iterated Kalman filters for simultaneous localization and mapping of autonomous mobile robots," *J. Intell. Rob. Syst*. **63**(3–4), 575–594 (2011).
38. K. Shojaei and A. M. Shahri, "Iterated Unscented SLAM algorithm for navigation of an autonomous mobile robot," **In**: *2008 IEEE/RSJ International Conference on Intelligent Robots and Systems*, Nice, France (2008).
39. L. Xu and B. Yao "Output feedback adaptive robust precision motion control of linear motors," *Automatica* **37**, 1029–1039 (2001).
40. K. Shojaei, "Saturated output feedback control of uncertain nonholonomic wheeled mobile robots," *Robotica* **33**, 87–105 (2015).